Marine Pollution Bulletin 231 (2026) 119926

Contents lists available at ScienceDirect

Marine Pollution Bulletin

journal homepage: www.elsevier.com/locate/marpolbul

Influence of mangrove zonation on dissolved trace metal dynamics in soils

Naïna Mouras [a,b,*], Maximilien Mathian [a], Sarah Louise Robin [a], Hugues Lemonnier [b,c], Cyril Marchand [a]

[a] Institute of Applied and Exact Sciences (EA7484), University of New Caledonia, Noumea, New Caledonia
[b] Ifremer, UMR 9220 ENTROPIE (IRD, Univ. Réunion, IFREMER, Univ. Nouvelle-Calédonie, CNRS), Noumea, New Caledonia
[c] MARBEC, Univ. Montpellier, CNRS, Ifremer, IRD, Montpellier, France

ARTICLE INFO

Keywords:
Porewater
Rhizophora stylosa
Avicennia marina
Salt-flat
Land-sea gradient

ABSTRACT

Mangrove soils play a key role in the cycling of trace metals (TM), yet the drivers controlling dissolved metal concentrations and distribution in porewaters remain poorly studied. Here, we investigate the distribution, dynamic, and controlling factors of dissolved TM along a land-sea gradient in the semi-arid mangrove of Bouraké (New Caledonia). Dissolved and solid-phase TM concentrations were measured in soils (0–30 cm), together with porewater chemistry, redox conditions, bulk density, and mineralogical composition (SEM-EDX). Solid metal stocks and dissolved to solid ratios were calculated to assess relative metal mobility. Dissolved TM concentrations exhibited strong spatial heterogeneity along the land-sea gradient, reflecting zonation-specific geochemical conditions. The landward salt-flat is the most oxidizing zone and contains abundant Fe-Ti oxides, resulting in the largest solid-phase metal stocks. The intermediate *Avicennia marina* stand is characterized by suboxic redox conditions and exhibits the highest dissolved Fe, Mn, Ni, and Co concentrations, indicating active Fe-Ti oxide dissolution. In contrast, the seaward *Rhizophora stylosa* stand is characterized by strong anoxia, pyritization, low dissolved metal concentrations, and the lowest solid-phase stocks, consistent with metal sequestration into sulfides. Overall, our results show that dissolved TM dynamics in mangrove soils is governed by the combined influence of redox dynamics, organic matter quantity, and mineralogical transformations. Because dissolved metals represent the most mobile and exportable fraction, this study highlights the necessity of considering porewater chemistry to assess metal cycling and export in mangrove.

1. Introduction

Mangrove forests form a key ecotone between land and sea, located in the intertidal zone of tropical and subtropical coastlines (Giri et al., 2011). Beyond their well-known role in carbon storage and source to adjacent ecosystems (Alongi, 2014; Donato et al., 2011; Kristensen et al., 2008), mangroves strongly influence the dynamic of trace elements along tropical coastlines. Mangrove soils are highly reactive and can contain high concentrations of dissolved trace metals (TM), which can be exported toward coastal waters through the tidal pumping process (Mori et al., 2019; Sadat-Noori and Glamore, 2019).

Mangrove soils act both as sinks and sources of TM depending on organic and physico-chemical conditions. Anoxic and organic-rich soils promote the precipitation and retention of metals either incorporated into sulphur mineral structure or adsorbed onto organic molecules (Luz-Santos et al., 2025; Mounier et al., 2001; Zhu et al., 2019). Conversely, variation in redox conditions may promote minerals dissolution and OM decomposition, which release TM into the porewater (Alongi et al., 1999; Marchand et al., 2006; Pérez et al., 2021) and then to the surface waters and creeks with the tidal movement (Holloway et al., 2016; Knoke et al., 2024; Sanders et al., 2015).

Dissolved TM in mangrove porewaters may have different origins. Tides and river inputs represent a minor contribution in preserved mangrove without direct anthropogenic input. Most dissolved metals originate from biogeochemical processes occurring within preserved mangrove soils. The dissolution of mineral phases, especially metal-bearing oxides, sulfides or clays, release their associated metals into mangrove soil porewater (Canfield, 1989). This dissolution often occurs when physico-chemical conditions change (Eh, pH, fluids chemical composition…). For instance, Fe- and Mn-oxyhydroxides can dissolve under suboxic conditions by bacteria for organic matter (OM) decomposition, and induce an accumulation of dissolved TM in porewater

* Corresponding author at: Institute of Applied and Exact Sciences (EA7484), University of New Caledonia, Noumea, New Caledonia.
E-mail address: naina.mouras@unc.nc (N. Mouras).

https://doi.org/10.1016/j.marpolbul.2026.119926
Received 9 March 2026; Received in revised form 18 May 2026; Accepted 24 May 2026
Available online 2 June 2026

(Nath et al., 2013; Taillefert et al., 2002; Thamdrup et al., 2000; Noël et al., 2014). In addition, OM decomposition can also release TM in porewater since some TM and OM can for complex in soils both in the solid and dissolved phases.

Although some studies have characterized total metal concentrations in mangrove soils and their accumulation in plant tissues (Bayen, 2012), only relatively few studies have focused on the dissolved metal pool in coastal wetlands, including mangrove porewaters (Alkhadher et al., 2023; Holloway et al., 2016; Sallan et al., 2023; Thanh-Nho et al., 2020). The question of the key drivers that can control its variability along a land-sea gradient also remains open in the literature. Where porewater studies exist, they often highlight strong temporal (tidal, seasonal) and biogeochemical coupling with dissolved OM (Holloway et al., 2016; Mori et al., 2019; Sadat-Noori and Glamore, 2019; Thanh-Nho et al., 2020). However, the links between soil mineralogy (Fe-oxyhydroxides, Fe-sulfides such as pyrite), organic carbon quantity (total organic carbon (TOC)/ dissolved organic carbon (DOC)), redox dynamics and dissolved metal concentrations remains underexplored, especially in semi-arid mangroves. Climatic conditions in this ecosystem differ from those in humid mangroves, with lower precipitation, higher daily temperature fluctuation, intense solar radiation and high (Adame et al., 2021; Ball, 1980). As a result, mangroves in semi-arid climates experience low humidity and hypersaline conditions, which strongly affect soil physico-chemical properties such as salinity, redox potential and metal speciation. The lack of freshwater inputs in semi-arid mangrove limits water mass exchanges, inhibits the flushing rate and increases the residence time of water in soil, which limits dissolved TM export out of the system. Furthermore, conditions during dry seasons may enhance porewater seepage, and induce organic matter decay, which favours TM release in the dissolved phase (Leopold et al., 2017). Semi-arid mangroves are distributed in subtropical zone and remain less studied than humid tropical systems (Adame et al., 2021). Moreover, most previous studies on TM dynamics in mangroves have focused on tropical mangroves, on the solid phase of metals rather than dissolved fractions, and on systems impacted by anthropogenic contamination. In contrast, semi-arid mangroves remain poorly studied despite their strong physico-chemical gradients, which may substantially influence dissolved TM behaviour and mobility. Furthermore, pristine mangrove systems receiving predominantly natural TM inputs remain largely unexplored, despite providing an opportunity to investigate baseline geochemical controls on dissolved metal dynamics without the overriding influence of anthropogenic sources.

The mangroves of New Caledonia provide a relevant setting to investigate dissolved TM dynamics under semi-arid conditions. On the west coast of the main island, tidal and salinity regimes govern species zonation and soils properties (Adame et al., 2021; Marchand et al., 2016, 2012). In this region, monospecific zones commonly occur along a land-sea transect: salt-flat (often with little or no vegetation), followed by *Avicennia marina* stands and, seaward, *Rhizophora* spp. (Duke et al., 2007). Reported porewater salinities and inundation regimes differ strongly between these zones (salt-flat: ~60–100 g L^{-1}; *A. marina*: ~35–70 g L^{-1}; *Rhizophora* spp.: ~5–40 g L^{-1}). In addition to its semi-arid climate, the geological context of New Caledonia makes its mangrove systems relevant for TM studies. Around one third of the island is covered by lateritic soils, which are naturally enriched in iron oxides and TM such as Ni, Co and Cr (Tardy and Roquin, 1992). As a consequence, most previous studies on New Caledonian mangroves have primarily focused on the impacts of mining activities, enhanced erosion, and the inputs of lateritic sediments on mangrove ecosystems (Bourgeois et al., 2020; Marchand et al., 2012; Robin et al., 2021). However, despite this extensive work on solid-phase metal accumulation and anthropogenic inputs, the key geochemical drivers controlling the distribution of dissolved TM in mangrove porewaters remain largely unexplored.

Given this context, understanding how soil mineralogy and organic carbon quantity (both dissolved and particulate) control dissolved TM concentrations and dynamics in mangrove porewaters is considered highly relevant for identifying the key geochemical drivers of metal cycling in mangrove soils. This process-based approach helps to better understand how dissolved TM behave in mangrove soils, including their distribution, bioavailability and potential export to coastal waters, especially in semi-arid systems, where strong physico-chemical gradients enhance these processes. The main objective of this study is to characterize the dynamics and drivers of dissolved TM in porewaters along a land-sea gradient in a semi-arid mangrove. Specifically, we aim to: (i) quantify dissolved TM concentrations in soil porewaters along salt-flat, *Avicennia marina* and *Rhizophora stylosa* stands; (ii) link these concentrations to soil properties, including mineralogy, TOC/DOC, and bulk density; (iii) estimate solid metal stocks (0–30 cm) to evaluate the metal storage capacity of each stand and calculate dissolved/solid ratios to assess relative mobility. By focusing on the dissolved phase and its connection to soil mineralogy and OM, this study seeks to clarify the processes that control dissolved TM dynamics in semi-arid mangroves and to assess their potential for coastal export.

2. Material & methods

2.1. Study site and sampling

The study was conducted in the semi-enclosed mangrove system of Bouraké, located on the West-coast of New Caledonia (21.946° S, 165.999° E; Fig. 1). This site represents a typical semi-arid mangrove environment of the South Pacific (Adame et al., 2021), characterized by a clear land-sea zonation of three main stands: salt-flat at the landward edge, *A. marina* stands in the intermediate stand, and *R. stylosa* forests closer to the lagoon. The entire mangrove covers approximately 2.5 km^2 and is dominated by *R. stylosa*, which accounts for about 76% of the total area.

This mangrove is connected to the lagoon by a narrow channel bordered by coral reefs (Fig. 1). In the center of the mangrove swamp are two pools whose water level varies with the tide. This configuration creates limited water exchange with the surrounding lagoon and generates pronounced salinity and redox gradients within the mangrove soils (Mouras et al., 2025a). The system lacks any major freshwater inputs, and its hydrology is mainly controlled by tidal pumping and evaporation. The tidal regime is semi-diurnal, with tidal ranges varying from ~0.6 m during neap tides to ~1.25 m during spring tides (Mouras et al., 2026). Tidal inundation frequency decreases along the land-sea gradient: *R. stylosa* stands are regularly flooded, *A. marina* stands are inundated mainly during spring tides, while salt-flat areas are only rarely reached by the highest tides (Marchand et al., 2016). This gradient in tidal inundation directly influences redox conditions, salinity, and organic matter inputs across stands (Mouras et al., 2025a). Such specific conditions result in Bouraké being an ideal natural laboratory to study the biogeochemical functioning of mangrove soils under semi-arid conditions.

The soils are underlain by volcano-sedimentary formations (Ullmann et al., 2014). Consequently, the geochemical composition of the soils primarily reflects autochthonous processes such as mineral weathering, eogenetic transformations, redox cycling, and OM degradation (Mouras et al., 2025a). The presence of coral fragments and carbonate-rich sands near the tidal channel also contributes to the geochemical diversity of the soil matrix.

Cores (30 cm) were collected at the end of the wet (June 2023) and dry (October 2023) seasons at the three stands along the land-sea transect (salt-flat, *A. marina*, *R. stylosa*) at low tide with a manual stainless-steel corer. Three cores were collected for each mangrove stands (Fig. 1). After being collected, cores were sectioned into three 10 cm layers (0–10, 10–20, 20–30 cm). Subsamples dedicated to TM analysis were collected at the center of each section. Samples were kept frozen until 48 h freeze-drying, then grounded with an agate pestle and mortar <80 μm. Around 1 g of material was used for TM analysis.

Before the solid samples collection, porewaters were extracted

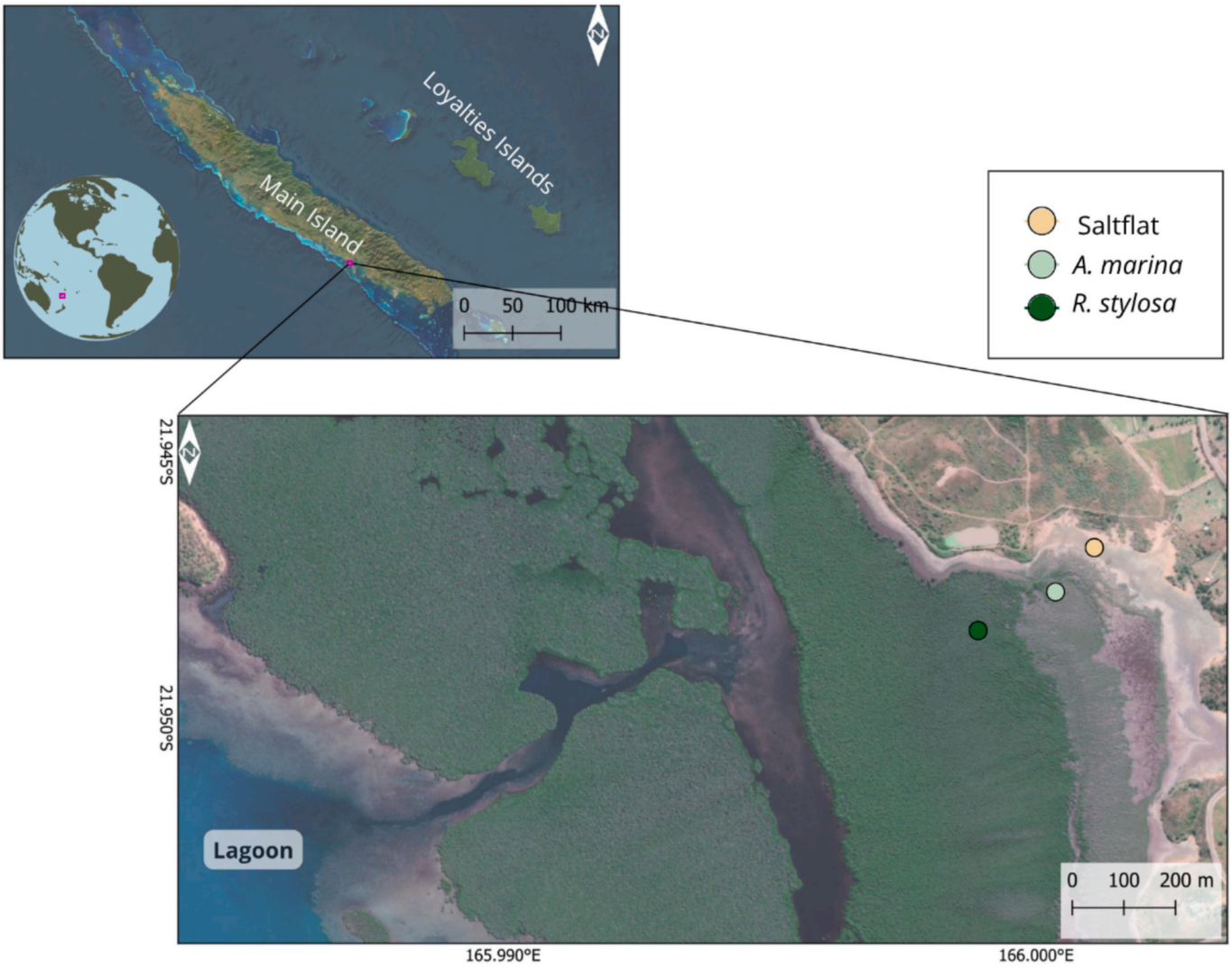

Fig. 1. Map of the Bouraké mangrove showing the three sampling stands (salt-flat, *Avicennia marina*, *Rhizophora stylosa*) and the location of the sediment cores collected in June and October 2023 (QGIS 3.28.6; ESRI satellite™, September 2025).

directly in the field using a Rhizon® soil moisture samplers (0.2 μm pore size, MOM-10 cm) inserted into each core section. Each sampler was connected to syringes previously cleaned in 10% HNO_3 baths, rinsed with ultrapure water, and stored in 0.1% HNO_3 until use. One Rhizon® sampler was inserted per 10 cm core section (0–10, 10220, 20–30 cm), and porewater was extracted from three replicate cores per stand. The use of Rhizon® samplers allowed direct in situ extraction of porewater, minimizing potential oxidation artifacts during sampling. Immediately after collection, porewater samples were filtered on the field through 0.2 μm cellulose acetate filters (Sartorius®). Subsamples for TM analysis were acidified with ultrapure HNO_3 (pH < 2) stored in acid-cleaned 15 mL metal-free polypropylene tubes (Labcon®). Aliquots for DOC analysis were acidified with HCl (pH < 2) and stored in pre-combusted glass vials at 4 °C in the dark until analysis (Mouras et al., 2025a). In situ salinity, pH, and redox potential (Eh) were measured on separate subsamples immediately after extraction using calibrated portable sensors. Eh measurements were performed at the center of each core section. Cores were collected away from crab burrows and large mangrove roots to limit the influence of microscale redox heterogeneity. Eh values were corrected to the standard hydrogen electrode (SHE) by adding +220 mV to readings obtained with an Ag/AgCl reference electrode. All sampling equipment was acid-cleaned and rinsed with ultrapure water prior to use. Samples were transported at 4 °C to the laboratory and stored in the dark at 4 °C until analysis.

2.1.1. Soil characteristics

Soil bulk density, TOC, and DOC data used in this study were previously published in (Mouras et al., 2025b) and were obtained from the same study sites, during the same sampling campaigns as the present TM investigation. They are used in this study to present the environmental characteristics of the studied mangrove stands. Briefly, bulk density was determined using a volumetric sampling method with a 20 cm^3 cylindrical syringe, and depth-specific values (0–10, 10–20, 20–30 cm) were used for stock calculations. A detailed description of sampling, analytical procedures and results is provided in Mouras et al. (2025a). Mean values for each stand are presented in Table 1, summarizing all physicochemical properties.

2.2. Analytical methods

2.2.1. Scanning electron microscopy (SEM)

Scanning Electron Microscopy (SEM) was used to observe the mineral composition and the petrographic organization of the soil samples from the three stands. Bulk dried soil fragments were placed on aluminium stubs using conductive carbon tape. Because the samples are electrically insulating, they were coated with a thin 4-nm carbon layer

Table 1
Mean values (± SD) of bulk density (g.cm^{-3}), pH, Eh, salinity, TOC (%), DOC (mg.L), clay (%), silt (%), and sand (%) in the soil of the 3 studied mangrove stands in Bouraké, New Caledonia. n: number of samples used to calculate mean values. Dataset described in Mouras et al. (2025a).

	Salt-flat (n = 18)	*A. marina* (n = 18)	*R. stylosa* (n = 18)
Bulk density (g. cm^{-3})	1.4 ± 0.11	1.04 ± 0.22	0.51 ± 0.05
pH	7.12 ± 0.4	6.7 ± 0.19	6.11 ± 0.15
Eh (mV)	300.56 ± 146.09	−21.96 ± 89.01	−114.33 ± 77.57
Salinity	102.78 ± 26.94	56.17 ± 2.81	45.94 ± 2.21
TOC (%)	1.31 ± 0.7	2.75 ± 1.49	9.44 ± 0.99
DOC (mg.L^{-1})	14.61 ± 3.27	30.43 ± 16.49	49.34 ± 31.66
Clay (%)	12.32 ± 8.56	13.44 ± 3.77	9.31 ± 3.88
Silt (%)	62.47 ± 23.37	75.35 ± 7.91	84.78 ± 4.85
Sand (%)	25.21 ± 28.69	11.2 ± 9.35	5.91 ± 6.17
Water content (%)	25.65 ± 4.29	39.78 ± 7.97	61.81 ± 2.18

using a Leica EM AC600 coater to prevent charge accumulation on the surface. Observations were performed with a JEOL JSM-IT300LV microscope equipped with an Oxford CAM 80 EDX detector at the Electronic Microscopy Platform (P2M) of the University of New Caledonia. All the measurement were performed, both using a Secondary Electron Detector (for sample organization) and a Backscattered Electron Detector (for metal-bearing minerals localisation) at 20 kV and an effective working distance of 10 mm. SEM images were used to describe soil texture and mineral associations, and EDX provided semi-quantitative elemental information on selected particles. EDX were analysed on the Aztec™ dedicated software.

2.2.2. Solid and dissolved traces metals (ICP-OES and ICP-MS)

Main element and TM concentrations in solid samples were determined for three replicates per stand. Powdered samples were analysed by the Analytical Service for Rocks and Minerals (SARM) of the French National Centre for Scientific Research (CNRS, France). Powdered samples (300 mg) were fused with 900 mg of ultra-pure $LiBO_2$ in Pt crucibles at 980 °C in an automatic tunnel oven for approximately 60 min (Carignan et al., 2001). After cooling, the fusion glass was dissolved in a HNO_3 (1 mol L^{-1}) - H_2O_2 (~0.5% v/v) - glycerol (~10% v/v) mixture. Five international geochemical reference materials (basalt BR, anorthosite AN-G, serpentinite UB-N, diorite DR-N, and granite GH) and procedural blanks were included in each analytical batch to monitor accuracy and precision. Element concentrations were quantified by ICP-OES and ICP-MS and are expressed in µg g^{-1} dry weight. Limits of determination and measurement uncertainties are detailed in Carignan et al. (2001) and are available on the SARM website (https://sarm.cnrs.fr/index.html/). In this article, the mean value of the chemical elements obtained from the three replicates is compared for each stand to discriminate their effect.

Dissolved TM were quantified at the Laboratory for Physical Chemistry of Traces, Ruđer Bošković Institute (Croatia). Concentrations of Al, V, Cr, Mn, Fe, Co, Ni, Cu, Zn, As, Rb, Sr, Mo, Cd, Sn, Ba, Pb and U in porewater samples were determined using an Agilent 8900 Inductively Coupled Plasma Mass Spectrometer (ICP-MS). To minimize matrix effects from salinity, samples were diluted prior to analysis with dilution factors adapted to the salinity of each sample, ranging from 20-fold (*R. stylosa* porewaters, salinity ~42–49) to 80-fold (salt-flat porewaters, salinity up to 156). Measurements were performed in helium collision mode. An internal standard (^{115}In, 10 µg L^{-1}) was added to all samples to correct for instrumental drift. Analytical accuracy was assessed using certified reference material CASS-6 (Nearshore Seawater Reference Material for Trace Metals, National Research Council Canada). Quality control included duplicate analyses of two CASS-6 standards and two additional QC samples from WEPAL-QUASIMEME interlaboratory tests, measured every 15 samples. Quantification was achieved using matrix-matched external calibration (20-fold diluted seawater, 0–10 ppb standards). Measured concentrations in QC materials were within 15% of the certified values.

2.2.3. Stocks and ratios

Elemental stocks were calculated from concentration (µg g^{-1}), bulk density (g cm^{-3}) and sampling depth (m). First, TM concentrations in µg g^{-1} were converted to stock per unit area (g m^{-2}) for a given sampling depth (D, m).

$$Stock\ (g\ m^{-2}) = concentration\ (\mu g\ g^{-1}) \times density\ (g\ cm^{-3}) \times D(m)$$

Then g m^{-2} values were converted to tonnes per hectare (t ha^{-1}), and stock results in t ha^{-1} were integrated over 30 cm depth to obtain a single value per stand.

Solid-phase metal stocks were normalized to titanium (Ti), a conservative and immobile element in soils (Taylor and McLennan, 1985), in order to correct for sediment dilution effects and to isolate true geochemical variations along the land-sea gradient.

Dissolved to solid ratios were calculated as the concentration of dissolved metals (µg L^{-1}) divided by solid-phase concentrations (µg g^{-1}), and are used here as an index of relative metal mobility across stands.

2.3. Statistics

All statistical analyses were performed using R software (version 4.0.3). Descriptive statistics were first calculated to summarize the dataset. To examine the combined effects of zonation (salt-flat, *A. marina*, *R. stylosa*), season (dry vs. wet), and soil depth (0–10 cm, 10–20 cm, 20–30 cm) on the overall geochemical dataset, including solid and dissolved TM concentrations and associated environmental variables (pH, Eh, salinity, grain size, TOC, and DOC), a permutational multivariate analysis of variance (PERMANOVA) was conducted using the adonis2 function from the vegan package. The analysis was based on Bray-Curtis dissimilarities calculated from fourth-root transformed data, with 999 permutations. A significance threshold of $p < 0.05$ was applied for all tests. This exploratory multivariate analysis indicated that zonation was the dominant structuring factor of the dataset, explaining 32% of the total variance. Pairwise PERMANOVA comparisons (pairwise.adonis2, 999 permutations) confirmed that all three stands differed significantly from each other (salt-flat vs. *A. marina*: $R^2 = 0.33$, $F = 17.9$, $p = 0.001$; salt-flat vs. *R. stylosa*: $R^2 = 0.46$, $F = 31.2$, $p = 0.001$; *A. marina* vs. *R. stylosa*: $R^2 = 0.42$, $F = 26.7$, $p = 0.001$). Based on this result, and in line with the objectives of this study, the presentation of results focused on stand-driven differences in TM concentrations and stocks.

Prior to univariate analyses of dissolved and solid TM concentrations, data normality and homogeneity of variance were assessed using Shapiro-Wilk and Levene's tests, respectively. When assumptions were met, one-way ANOVA was applied, followed by Tukey's HSD post-hoc tests. For non-normal or heteroscedastic data, non-parametric Kruskal-Wallis tests were used, with pairwise Wilcoxon rank-sum tests for post-hoc comparisons.

For solid-phase TM, spearman rank correlation matrices were calculated to identify relationships among elements and detect collinearity. Because many TM exhibited strong co-variation due to shared mineralogical hosts or similar geochemical behaviour, elements showing high collinearity ($\rho > 0.8$) were excluded to reduce redundancy and avoid overweighting correlated variables in multivariate analyses. Following this variable selection, a principal component analysis (PCA) was performed on the reduced dataset to explore spatial structuring of solid-phase TM across stands.

3. Results

3.1. Dissolved trace metal concentrations

Dissolved TM concentrations showed clear spatial trends along the land-sea gradient from the salt-flat to *R. stylosa* (Table 2). As(d) increased seaward from 3.98 ± 1.19 μg L^{-1} in the salt-flat to 11.7 ± 11.9 μg L^{-1} under *R. stylosa*. Ba(d) followed the same trend.

In contrast, several elements decreased seaward, such as Cd, Co, Cu, Mo, Ni, Sn, Sr, V and Zn (Table. 2). Mo(d) concentrations were significantly higher in the salt-flat (20.5 ± 7.7 μg L^{-1}) and declined toward the seaward stands, reaching 5.2 ± 6.3 μg L^{-1} under *R. stylosa* ($p < 0.05$, Kruskal-Wallis). Zn(d) also decreased progressively, from 280 ± 149 μg L^{-1} in the salt-flat to lower levels under *A. marina* and *R. stylosa*. Ni(d) was slightly enriched in the salt-flat (23.8 ± 12.5 μg L^{-1}) compared to both mangrove stands (≈10 μg L^{-1}).

A group of elements (Fe, Mn, U, Cr and Pb) displayed a distinct maximum under *A. marina*. Fe(d) and Mn(d) showed their highest concentrations in this stand (11,945 ± 16,566 and 3798 ± 2577 μg L^{-1}, respectively) compared to much lower levels in the salt-flat (19 ± 9 and 467 ± 591 μg L^{-1}) and moderate values under *R. stylosa* (1159 ± 1916 and 276 ± 127 μg L^{-1}) ($p < 0.05$, Kruskal-Wallis). U(d) and Cr(d) followed a similar pattern, with a maximum mean value observed under *A. marina* (18.3 ± 43.1 μg L^{-1} and 3.31 ± 2.21 μg L^{-1}, respectively), although this pattern is characterized by large variability and was not statistically significant.

3.2. Solid trace metals distribution

Because many solid TM exhibited similar patterns and strong intercorrelations, a variable selection was applied prior to data presentation. Elements with high collinearity ($\rho > 0.8$) were excluded to avoid redundancy, and Table 3 therefore focuses on TM with distinct geochemical behaviour, others TM are presented in table S1. The average concentration of TM (As, Cd, Co, Cr, Cs, Cu, In, Mo, Ni, Sb, Sc, Sr, U, W, Zn, Ce, Al, Mn, Mg, Ca, Na, K, Ti, P, V) are presented in Table 3. As dissolved compartment, solid-phase TM concentrations showed distinct patterns along the land-sea gradient.

Cr, Ni, Mo and U showed an increase from the salt-flat to *R. stylosa*. Cr rose from 150 ± 39 μg g^{-1} to 229 ± 19 μg g^{-1}, while Ni concentrations were lower in the salt-flat (67 ± 26 μg g^{-1}) and increased significantly under both mangrove stands, reaching 98 μg g^{-1} under the two mangrove stands. Mo and U also increased strongly seaward, reaching their highest values under *R. stylosa*.

In contrast, several elements were the most concentrated in the salt-flat and declined toward the sea. This was the case for As, Co, Cs, Cu, Mn, Ca, Ti, In, and P. For example, Mn decreased from 350 ± 222 μg g^{-1} in the salt-flat to 163 ± 71 μg g^{-1} under *R. stylosa*, and Ti decreased significantly from 5144 ± 767 to 3966 ± 547 μg g^{-1} ($p < 0.05$, Kruskal-Wallis).

A distinct group of elements reach its maximum in the intermediate stand *A. marina*: Sc, Sr, Zn, Ce, Al, Mg, K, Cd, V and W. For instance, Al reached 63,251 ± 2668 μg g^{-1} under *A. marina*, higher than in the salt-flat (60,589 ± 6067 μg g^{-1}) and *R. stylosa* (54,317 ± 6394 μg g^{-1}).

Sb remained low and showed little spatial variation across stands. Fe also exhibited low variation along the gradient, remaining relatively stable between the salt-flat and *A. marina* and *R. stylosa*. Ca showed no clear tendency across intertidal gradient. Na behaved differently from other major elements, with its highest concentrations found under *R. stylosa*.

Table 2
Dissolved trace metal concentrations (μg L^{-1}, mean ± SD) in porewaters of the three stands along the land-sea gradient: salt-flat, *A. marina*, and R. stylosa. Different letters indicate significant differences among stands (Kruskal-Wallis test followed by Dunn post-hoc test with Bonferroni correction, $p < 0.05$).

Dissolved TM (μg L^{-1})	Salt-flat ($n = 18$)	*A. marina* (n = 18)	*R. stylosa* (n = 18)
Increasing from the land to sea			
As(d)	3.98 ± 1.19^{a}	7.34 ± 12.2^{a}	11.7 ± 11.9^{a}
Ba(d)	170 ± 67.8^{a}	192 ± 92.0^{a}	205 ± 134^{a}
Decreasing from land to sea			
Cd(d)	0.0957 ± 0.068^{a}	0.0187 ± 0.0173^{b}	7e-03 ± 4.72e-03^{b}
Co(d)	6.53 ± 9.92^{a}	1.83 ± 1.96^{ab}	1.06 ± 1.19^{b}
Cu(d)	2.97 ± 0.979^{a}	0.724 ± 0.462^{b}	0.310 ± 0.212^{b}
Mo(d)	20.5 ± 7.69^{a}	16.0 ± 24.3^{b}	5.24 ± 6.25^{c}
Ni(d)	23.8 ± 12.5^{a}	10.1 ± 10.0^{b}	10.1 ± 10.5^{b}
Sn(d)	0.361 ± 0.103^{a}	0.270 ± 0.0813^{a}	0.135 ± 0.0387^{b}
Sr(d)	1.48e+04 ± 3930^{a}	1.19e+04 ± 865^{a}	9560 ± 465^{b}
V(d)	5.22 ± 2.08^{a}	4.60 ± 5.59^{b}	2.12 ± 0.661^{b}
Zn(d)	280 ± 149^{a}	208 ± 164^{a}	105 ± 119^{b}
Maximum in intermediate stand			
Cr(d)	2.11 ± 1.70^{ab}	3.31 ± 2.21^{a}	1.70 ± 0.553^{b}
Fe(d)	19.3 ± 9.11^{c}	1.19e+04 ± 1.66e+04^{a}	1160 ± 1920^{b}
Mn(d)	467 ± 591^{b}	3800 ± 2580^{a}	276 ± 127^{b}
Pb(d)	0.578 ± 0.332^{a}	0.599 ± 0.403^{a}	0.300 ± 0.273^{b}
U(d)	11.3 ± 5.56^{a}	18.3 ± 43.1^{a}	1.57 ± 1.83^{b}
No clear trend			
Al(d)	41.2 ± 32.7^{a}	21.8 ± 12.6^{a}	32.8 ± 30.9^{a}
Rb(d)	187 ± 58.0^{a}	111 ± 12.4^{c}	125 ± 14.4^{b}

Table 3
Mean (±SD) concentrations of trace metals (μg g^{-1}, dry weight) in the solid phase of mangrove soils from the three stands. Values are averages of 18 replicates per stand. Different letters indicate significant differences among stands (Kruskal-Wallis test followed by Dunn post-hoc test with Bonferroni correction, $p < 0.05$).

TM (μg.g^{-1})	Salt-flat ($n = 18$)	*A. marina* (n = 18)	*R. stylosa* (n = 18)
Increasing from the land to sea			
Cr	150 ± 39.1^{c}	211 ± 77.3^{b}	229 ± 19.1^{a}
Mo	2.99 ± 1.11^{b}	3.03 ± 1.43^{b}	7.38 ± 2.66^{a}
Ni	67.4 ± 25.6^{b}	98.0 ± 31.3 a	98.7 ± 9.52^{a}
U	1.56 ± 0.336^{c}	2.75 ± 2.32^{b}	4.50 ± 1.89^{a}
Decreasing from land to sea			
As	20.7 ± 5.54^{a}	19.1 ± 6.01^{a}	10.4 ± 4.94^{b}
Co	15.9 ± 8.43^{a}	14.5 ± 1.82^{a}	11.4 ± 1.30^{b}
Cs	3.56 ± 0.307^{a}	2.93 ± 0.325^{b}	1.74 ± 0.126^{c}
Cu	21.1 ± 4.15^{a}	20.3 ± 2.54^{a}	17.6 ± 2.03^{b}
In	0.0454 ± 4.17e-03^{a}	0.0466 ± 5.2e-03^{a}	0.0293 ± 7.34e-03^{b}
Mn	350 ± 222^{a}	264 ± 162^{a}	163 ± 71.4^{b}
P	364 ± 91.0^{a}	364 ± 47.3^{a}	332 ± 78.0^{a}
Ti	5140 ± 767^{a}	5010 ± 343^{a}	3970 ± 547^{b}
Maximum in intermediate stand			
Al	6.06e+04 ± 6070^{b}	6.33e+04 ± 2670^{a}	5.43e+04 ± 6390^{b}
Cd	0.0318 ± 0.0105^{ab}	0.0362 ± 7.67e-03^{a}	0.0252 ± 3.98e-03^{b}
Ce	23.8 ± 12.4^{b}	24.2 ± 2.09 ^{a}	19.0 ± 0.988^{b}
K	8800 ± 1240^{b}	9990 ± 1040^{a}	8530 ± 1580^{b}
Mg	1.24e+04 ± 4810^{a}	1.32e+04 ± 2820^{a}	1.25e+04 ± 3880^{a}
Sc	17.2 ± 1.27^{a}	18.4 ± 1.51^{a}	16.0 ± 1.01^{b}
Sr	124 ± 14.9^{ab}	135 ± 15.9^{a}	115 ± 8.58^{b}
V	133 ± 15.5^{a}	134 ± 17.6 ^{a}	87.1 ± 6.09^{b}
W	0.433 ± 0.0382^{b}	0.495 ± 0.0658^{a}	0.472 ± 0.0971^{ab}
Zn	51.9 ± 4.38^{b}	58.0 ± 4.03^{a}	49.3 ± 7.98^{b}
No clear trend			
Ca	5990 ± 1420^{a}	5930 ± 785^{a}	6200 ± 1340^{a}
Fe	4.37e+04 ± 4540^{a}	4.4e+04 ± 4440^{a}	4.37e+04 ± 5300^{a}
Na	3.51e+04 ± 4320^{b}	3.45e+04 ± 3220^{b}	3.93e+04 ± 4560^{a}
Sb	0.374 ± 0.0587^{a}	0.396 ± 0.0744^{a}	0.316 ± 0.086^{a}

3.2.1. Multivariate analysis of solid-phase metal composition

Collinearity among elements was first evaluated, and strongly correlated variables ($\rho > 0.8$) were removed, resulting in the exclusion of 27 elements (Pr, Nd, Tb, Gd, Yb, Ho, Er, Dy, La, Lu, Y, Sm, Hf, Tm, Nb, Eu, Ga, Rb, Be, V, Ba, Th, Si, Zr, Pb, Ta, Ge; Table.S1). A PCA performed on the remaining dataset showed that the first two components explained 27.6% and 13.4% of the total variance (Fig. 2). Along the first axis, *R. stylosa* samples were clearly separated from *A. marina* and salt-flat soils. Mo, Na, Ni, U, and Cr were associated with the *R. stylosa* group, whereas the remaining elements were linked to the salt-flat and *A. marina* stands. The second axis was mainly driven by major elements such as Mg, Ca, K and P, which were associated with the negative side of this axis, while several trace metals (e.g., Zn, Sc, Ce, In) were positively associated with it.

Overall, the three stands exhibit distinct solid-phase metal signatures along the land-sea gradient. Salt-flat are dominated by Fe and Ti oxides, with the highest Ti concentrations. *A. marina* soils show higher concentrations of Ni, Co, Cr, Cu, and Zn compared to salt-flat. *R. stylosa* soils are characterized by elevated Mo, Cr, Ni, U and Na concentration. These results highlight a clear spatial pattern of metal distribution in the solid phase across the mangrove gradient.

3.3. Trace metals stocks in the 3 studied stands

3.3.1. Absolute stocks of trace metals

Only TM with the highest concentrations and representative of the main geochemical trends are presented here (Fe, Ti, Ni, Cu, Mn, Cr, Co, Al and Mo; Table 4). Stock estimates for the remaining elements are provided in the Supplementary material (Table S2).

TM stocks in the upper 30 cm of the 3 studied mangrove soils exhibited a clear decrease along the land-sea gradient (Table 4). In the salt-flat, Fe and Al stocks were the highest, reaching 182.6 and 253.3 t ha^{-1}, respectively, followed by Ti (21.5 t ha^{-1}), Ni (0.28 t ha^{-1}), Mn (1.49 t ha^{-1}), Co (0.07 t ha^{-1}). The *A. marina* stand showed slightly lower stocks for most TM, with Fe at 137.4 t ha^{-1}, Al at 197.2 t ha^{-1}, Ti at 15.5 t ha^{-1}, Ni at 0.29 t ha^{-1}, Mn at 0.8 t ha^{-1}. In the *R. stylosa* stand, stocks were lower, with Fe and Al at 67.3 and 83.2 t ha^{-1}, Ti at 6.1 t ha^{-1}, Ni at 0.15 t ha^{-1}, Mn at 0.25 t ha^{-1}. Other metals (Cu, Cr, Mo) showed a similar decreasing trend from the salt-flat to the seaward *R. stylosa* stand (Table 4).

3.3.2. Normalized stock ratios (Fe/Ti and Ni/Ti)

To compare the relative distribution of elements regardless of soil

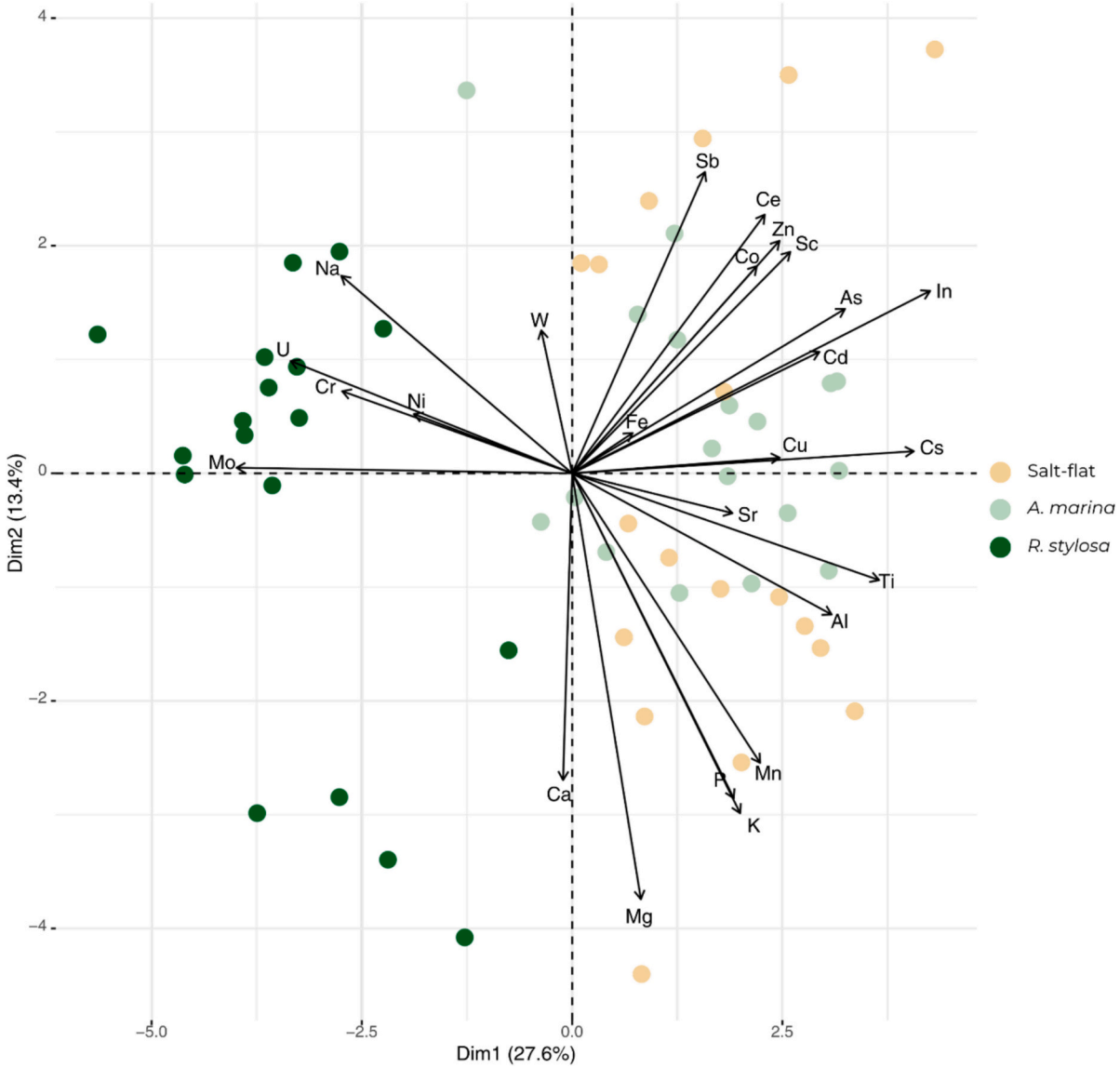

Fig. 2. Principal component analysis (PCA) based on solid-phase metal concentrations in soils from the three mangrove stands.

Table 4
Trace metal stock of selected elements in the soils of the 3 studied mangroves stand in Bouraké New Caledonia. Values are mean ± SD ($n = 3$ sites per stand, averaged over seasons) Stock were calculated using metal concentrations and bulk density for each sample, and then integrated on 30 cm depth. Different letters indicate significant differences among stands (Kruskal-Wallis test followed by Dunn post-hoc test with Bonferroni correction, $p < 0.05$). Stocks of other elements are presented in Fig. S2.

Stock (t ha)	Salt-flat (n = 3)	*A. marina* (n = 3)	*R. stylosa* (n = 3)
Al	253.309 ± 3.172^{b}	197.191 ± 22.727^{ab}	83.201 ± 7.619^{a}
Co	0.066 ± 0.017^{b}	0.045 ± 0.007^{ab}	0.018 ± 0.002^{a}
Cr	0.631 ± 0.047^{a}	0.630 ± 0.061^{a}	0.351 ± 0.026^{a}
Cu	0.088 ± 0.009^{b}	0.064 ± 0.011^{ab}	0.027 ± 0.003^{a}
Fe	182.588 ± 8.826^{b}	137.404 ± 15.276^{ab}	67.262 ± 4.799^{a}
Mn	1.488 ± 0.255^{b}	0.800 ± 0.093^{ab}	0.247 ± 0.083^{a}
Mo	0.012 ± 0.002^{a}	0.009 ± 0.001^{a}	0.011 ± 0.001^{a}
Ni	0.283 ± 0.026^{a}	0.294 ± 0.032^{a}	0.152 ± 0.011^{a}
Ti	21.466 ± 1.200^{b}	15,520 ± 1.001^{ab}	6.073 ± 0.679^{a}

mass, stock ratios were normalized to titanium (Ti) (Fig. 3). The Fe/Ti ratio showed a clear increase from land to sea, ranging from ~15–17 in the salt-flat to ~23 in the *R. stylosa* stand, while *A. marina* displayed intermediate values. The Ni/Ti ratio exhibited a similar gradient, with the highest values in *R. stylosa* (around 0.05) and *A. marina* (around 0.04), contrasting with lower ratios in the salt-flats (around 0.025). These trends highlight clear stand-related differences in the relative enrichment of Fe and Ni along the land-sea gradient. Only Ni and Fe are presented in the Fig. 3, other stock/Ti are presented in Supplementary material (Fig. S3).

3.4. Dissolved to solid trace metal ratios

Dissolved to solid ratios of TM showed four distinct patterns along the land-sea gradient (Table 5). Fe(d)/Fe and Mn(d)/Mn ratios peaked under *A. marina* (2.9×10^{-1} gL^{-1} and 1.7×10^{1} gL^{-1}, respectively), exceeding those in the salt-flat and *R. stylosa*. These maxima reflect a release of Fe and Mn into porewaters in this intermediate stand.

Most TM showed their highest ratios in the salt-flat, followed by a decrease toward *R. stylosa*. This was the case for Ni, Zn, Mo, Co, Cu, Cr, U, V and Cd. For instance, Ni(d)/Ni decreased from 0.41 gL^{-1} in the salt-flat to ~0.10 gL^{-1} in both mangrove stands, and Cd(d)/Cd dropped from 2.97 gL^{-1} in the salt-flat to 0.28 gL^{-1} under *R. stylosa*.

Table 5
Ratios of dissolved to solid concentrations of selected trace metals in porewaters and corresponding soils from the three mangroves stands (salt-flat, *A. marina*, R. stylosa). Different letters indicate significant differences among stands (Kruskal-Wallis test followed by Dunn post-hoc test with Bonferroni correction, $p < 0.05$).

Dissolved/solid (g L^{-1})	Salt-flat	*A. marina*	*R. stylosa*
Increasing from the land to sea			
As(d)/As	0.21^{b}	0.34^{ab}	1.3^{a}
Ba(d)/Ba	0.61^{b}	0.97^{b}	2.4^{a}
Pb(d)/Pb	0.050^{a}	0.071^{a}	0.18^{a}
Decreasing from land to sea			
Cd(d)/Cd	3.0^{a}	0.56^{b}	0.28^{b}
Co(d)/Co	0.46^{a}	0.13^{a}	0.094^{a}
Cr(d)/Cr	0.016^{ab}	0.016^{a}	0.0075^{b}
Cu(d)/Cu	0.14^{a}	0.036^{b}	0.018^{b}
Mo(d)/Mo	7.9^{b}	4.4^{b}	0.68^{a}
Ni(d)/Ni	0.41^{a}	0.11^{b}	0.099^{b}
U(d)/U	7.4^{b}	4.1^{b}	0.38^{a}
V(d)/V	0.039^{a}	0.037^{b}	0.025^{b}
Zn(d)/Zn	5.4^{b}	3.6^{ab}	2.0^{b}
Maximum in intermediate stand			
Fe(d)/Fe	4.0×10^{-4b}	2.9×10^{-1a}	2.7×10^{-2b}
Mn(d)/Mn	1.5^{b}	1.7×10^{1a}	1.9^{b}
No clear trend			
Al(d)/Al	6.8×10^{-4a}	3.4×10^{-4b}	6.3×10^{-4ab}
Rb(d)/Rb	5.1^{b}	2.6^{a}	4.1^{b}
Sr(d)/Sr	1.2×10^{2a}	88^{b}	84^{b}

A smaller group of elements showed the opposite pattern, with minimum ratios in the salt-flat and maximum values under *R. stylosa*. As (d)/As increased from 0.21 gL^{-1} in the salt-flat to 1.35 gL^{-1} under *R. stylosa*, while Ba(d)/Ba and Pb(d)/Pb followed the same trend.

A few elements showed limited variation along the transect. Al(d)/Al remained extremely low (10^{-4}–10^{-3} range) and relatively constant across stands. Sr(d)/Sr and Rb(d)/Rb varied only slightly and showed no consistent land-sea trend.

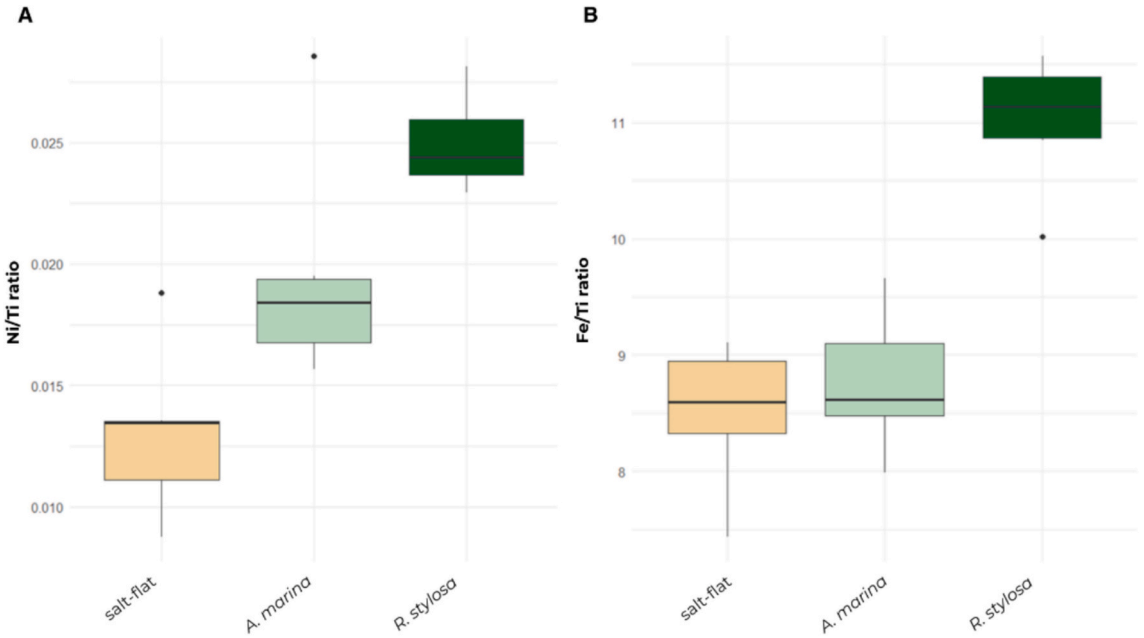

Fig. 3. Boxplots of Fe/Ti (A) and Ni/Ti (B) ratios in mangrove soils across the land-to-sea gradient (salt-flat, *A. marina*, R. stylosa).

3.5. Soil mineralogy description

SEM-EDX analyses revealed clear mineralogical contrasts along the land-sea transect (Fig. 4). In the salt-flat soils, dense aggregates of Fe and Fe-Ti oxides were dominant metal bearing-minerals (Fig. 4a) and the EDX spectra showed strong signals suggesting Ilmenites (Fig. S1). Few sulfates with incorporated Fe were observed but no pyrites. Feldspars and quartz grains were covered by a thin mineral coating (halite, oxides and silicates) and exhibited small signs of surface corrosion and partial dissolution. Note that few grains of chromite were observed at the SEM, but they were particularly rare (Fig. S1).

In the *A. marina* stand, mixed metal-bearing mineral assemblages were observed, combining residual oxides, specifically Ilmenite displaying pronounced dissolution features, with dispersed pyrite grains (Fig. 4b). Pyrites displayed subhedral to framboidal morphologies, marking more reducing conditions than in the salt-flats. EDX spectra occasionally showed small Ni and Cu peaks, suggesting minor metal incorporation as traces into the sulphide structures (Fig. S1).

Under *R. stylosa*, soils contained abundant framboidal pyrites, sometimes forming complex aggregates at depth, but no traces of Ilmenite nor Fe oxides were observed at the SEM scale (Fig. 4c). These minerals are generally linked to organic-rich grains, hosting biofilm and/or wood fragments (Fig. S2). Whereas the two first stands displayed in majority silicates or oxides grains covered by a more or less thick coating hosting reactive minerals (phyllosilicates, oxyhydroxides…), this last stand display particularly grains composed by a complex assemblage of OM, sulphides, silicates (including clays) and halite. EDX spectra showed clear Fe-S peaks with consistent, yet small, Ni and Cu signals, reflecting metal coprecipitation under sustained anoxic conditions.

The multivariate analysis (PCA) revealed a clear clustering of samples according to vegetation type, indicating strong stand-driven geochemical structuring (Fig. 5). Salt-flat samples were positioned on the positive side of PC1 and were associated with higher salinity, pH and Eh, together with dissolved Ni, Sn, Zn, Cu and Co. *A. marina* samples occupied an intermediate position along the PCA axes and grouped with dissolved Fe and Mn, as well as Al and Sc. *R. stylosa* samples formed a separate cluster on the negative side of PC1 and were mainly associated

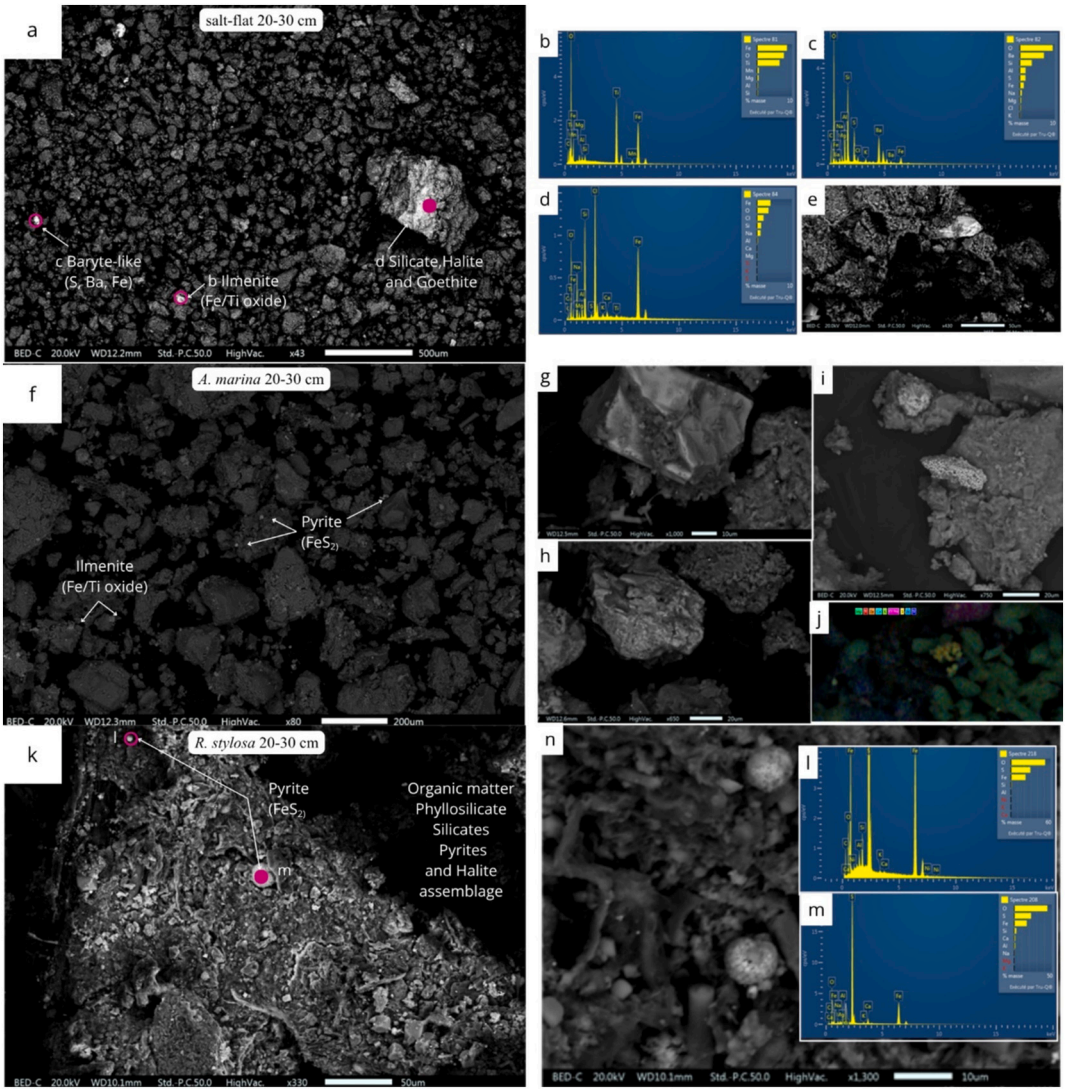

Fig. 4. SEM-EDX observations of soil samples from the three mangrove stands (20–30 cm depth). Salt-flat: (a) General view showing a sandy matrix dominated by quartz and feldspar grains with Fe-Ti oxides (ilmenite) and rare barite-like sulfate phases (b-d) EDX spectra of the main mineral phases identified (ilmenite, barite-like sulfate, silicate-halite-goethite assemblage); (e) detail of an ilmenite grain. *A. marina*: (f) General view showing less abundant and partially dissolved ilmenite grains with a thicker organo-mineral coating; (g-h) partially dissolved ilmenite grains; (i) pyrite crystals; (j) EDX elemental map showing co-occurrence of pyrite and anhydrite. R. stylosa: (k) General view of a representative grain assemblage composed of organic matter (including biofilms; Appendix S2), silicates, pyrite, and halite; (l-m) EDX spectra of pyrite crystals; (n) pyrite aggregates. Overall pattern of variability.

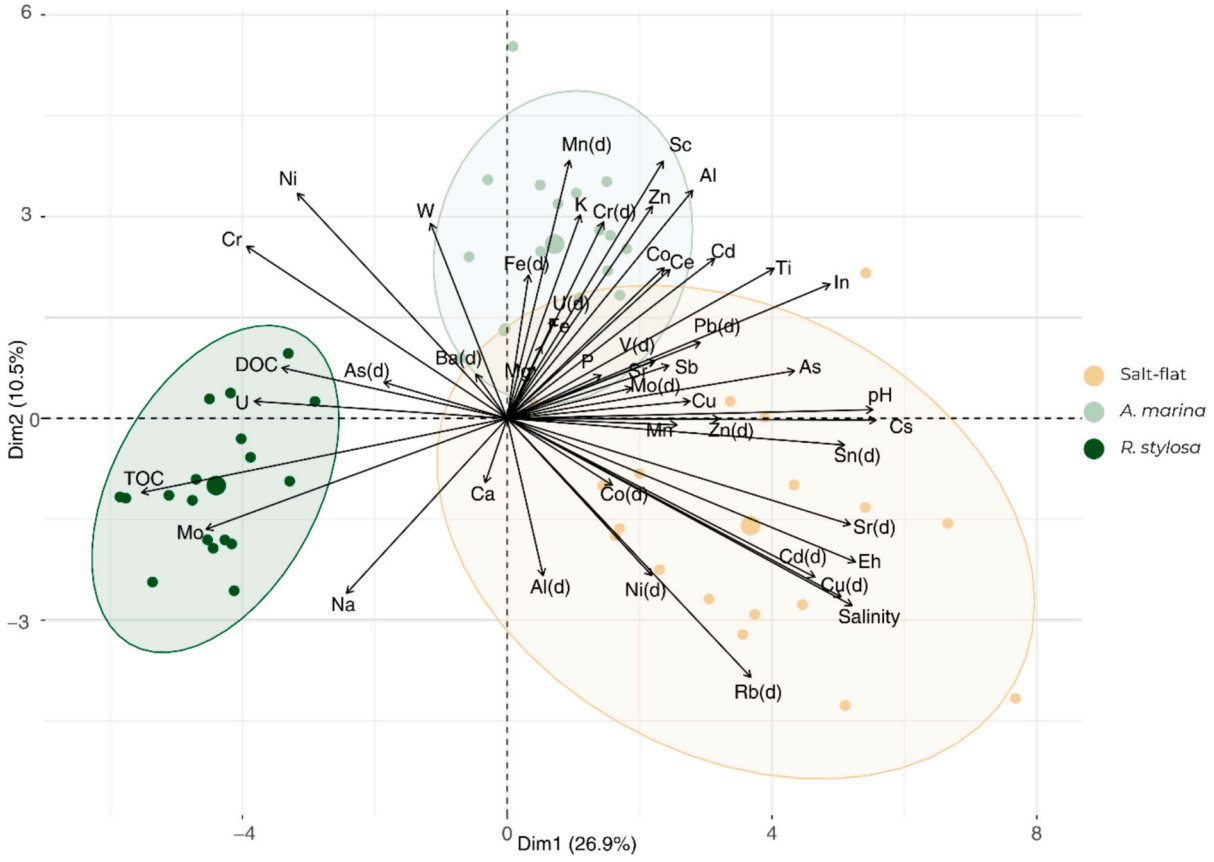

Fig. 5. Biplot of principal component analysis (PCA) (Dim 1: 26.9%, Dim 2: 10.5%) with K-means Clustering (K = 3).

with dissolved Mo, U and As, together with higher DOC and silt content. These patterns indicate that each stand is characterized by a distinct multivariate geochemical signature.

4. Discussion

4.1. Dissolved trace metal concentration across mangrove sites worldwide

Dissolved TM concentrations in Bouraké porewaters were within the upper range of values reported for mangrove worldwide, particularly for Fe, Mn, Ni and Co (Table 6). Dissolved Fe concentrations reached very high levels under *A. marina* (up to 11,945 μg L^{-1}), whereas lower concentrations were measured in several mangrove soils, such as those in Brazil (up to 4860 μg L^{-1}; Knoke et al., 2024), in Australia (up to 5640 μg L^{-1}; Sadat-Noori and Glamore, 2019), and in Vietnam (up to 2429 μg L^{-1}; Thanh-Nho et al., 2020). However, one study reported substantially higher Fe concentrations, reaching 19,871–64,277 μg L^{-1} in Island of Pai Matos (Brazil; Otero et al., 2009), highlighting the wide variability of dissolved Fe concentrations among mangrove systems worldwide. Similar patterns were observed for Mn, which ranged from 467 to 3798 μg L^{-1}, exceeding values reported in Vietnam (1523–2891 μg L^{-1}; Thanh-Nho et al., 2020), in Australia (275–483 μg L^{-1}; Holloway et al.,

Table 6
Mean concentrations of dissolved trace metal element in mangrove soils' porewaters in this study compared with the literature.

Study	Reference	Fe (μg L^{-1})	Mn (μg L^{-1})	Co (μg L^{-1})	Ni (μg L^{-1})	Cd (μg L^{-1})	Pb (μg L^{-1})
This study		19.33–11,945	467–3798	1.06–6.53	10.09–23.8	0.01–0.1	0.3–0.6
Vietnam	(Thanh-Nho et al., 2020)	1203–2429	1523–2891	9.4–5.7	9.0	–	–
Australia	(Holloway et al., 2016)	30–19,400	275–483	–	–	–	–
	(Sadat-Noori and Glamore, 2019)	up to 5640	9.3	–	–	–	–
Brazil	(Otero et al., 2009)						
	Avicennia	up to 19,871	2307–5936	–	–	–	–
	Rhizophora	up to 64,277	1319–8135	–	–	–	–
	(Knoke et al., 2024)	4860	1430	–	–	–	–
China	(Man et al., 2004)	–	–	–	–	0.3–121.1	2.6–105.6
New Caledonia	(Marchand et al., 2016)	3351	1099		58.7–1761	–	–
New Caledonia	(Marchand et al., 2012)						
Ultrabasic	Salt-flat	928	345	32.7	786	–	–
Ultrabasic	*A. marina*	1001	666	8.2	300	–	–
Ultrabasic	R. stylosa	428	666	34.9	730	–	–
New Caledonia	(Robin et al., 2021)						
Ultrabasic	*A. marina*	56,948	713	65	331	–	11
Ultrabasic	*R. stylosa*	57,790	2745	127	358	–	16
Non-ultrabasic	*A. marina*	8376	537	153	98	–	8
Non-ultrabasic	*R. stylosa*	135	323	73	113	–	7

2016), and in most Brazilian mangroves (1319–8135 μg L^{-1}; Otero et al., 2009). Dissolved Ni (10–24 μg L^{-1}) and Co (1–6 μg L^{-1}) also fall within the upper range of global values, reflecting the natural enrichment of New Caledonian soils in these TM (Kierczak et al., 2021; Marchand et al., 2012).

Even though, Bouraké is located within a non-ultrabasic watershed, dissolved Fe and Ni concentrations remain relatively high compared to global averages (Table 6). This pattern likely reflects the generally elevated geochemical background of New Caledonian soils and marine sediments, which are naturally enriched in Fe, Ni, Cr, and Mn (Beliaeff et al., 2011). Fe concentrations in Bouraké remain below those measured in ultramafic-dominated mangroves of New Caledonia, where Fe in porewaters may exceed 50,261 μg L^{-1} beneath *R. stylosa* (Noël et al., 2014), or 56,948 μg L^{-1} beneath *A. marina* (Robin et al., 2021), but they are slightly higher than values from non-ultramafic sites (8376 μg L^{-1}; Robin et al., 2021).

In this context, these elevated dissolved observed in Bouraké may partly reflect the influence of ultramafic-derived material in the region. While the Bouraké watershed is mainly dominated by sedimentary formations (Ullmann et al., 2014), several studies have shown that metal-rich particles from nearby ultramafic soils can be transported to coastal systems by lateral coastal current from the southeast (Douillet et al., 2001; Fernandez et al., 2006; Marchand et al., 2012; Maurizot et al., 2020; Ouillon et al., 2010).

In contrast, several dissolved TM concentrations such as Cd and Pb are low in Bouraké (0.01–0.1 μg L^{-1} and 0.3–0.6 μg L^{-1}, respectively). Much higher levels have been reported in mangroves impacted by anthropogenic inputs, such as by discharge of domestic and industrial wastes in China (Cd: 0.3–121 μg L^{-1}; Pb: 2.6–105 μg L^{-1}; (Man et al., 2004) or in urban mangroves of New Caledonia (Pb: 11–16 μg L^{-1}; Robin et al., 2021). This contrast highlights the difference between metals sourced from natural soil erosion, rarely enriched in Pb, and those linked to human activities, with Bouraké considered as a relatively preserved mangrove influenced by natural geochemistry rather than anthropogenic contamination.

Although these comparisons provide useful context, dissolved TM data from mangrove porewaters remain globally limited, making direct comparisons across sites difficult. Besides, the soil substrate composition as well as the nature of terrigenous sediments inputs in the system have a critical impact on the mangrove soil chemistry, solid and dissolved. In Bouraké, some dissolved metals may originate from a combination of hydrodynamic inputs, while others likely result from local processes such as mineral dissolution or OM diagenesis (discussed in the section below). These processes are strongly influenced by the geochemical characteristics of each stand along the intertidal gradient, which regulate metal dynamics in the soils.

4.2. Stand-driven geochemical control of trace metal distributions

The spatial behaviour of dissolved TM in Bouraké is strongly shaped by stand-specific geochemical conditions along the land-sea gradient. A previous study on this site demonstrated that tidal immersion and OM gradient both control redox conditions from anoxic beneath *R. stylosa* to oxic and evaporative conditions in the salt-flat (Mouras et al., 2025a). Such zonation, typical of semi-arid mangroves, has also been reported as a major driver of solid TM partitioning and transformation in New Caledonian mangroves, including deposition of oxyhydroxides, then dissolution by bacteria for the decomposition of OM, adsorption by reactive minerals (phyllosilicates/oxyhydroxides) and OM, or trapping into pyrite during sulfato-reduction processes (Marchand et al., 2012; Noël et al., 2014). The differences observed between stands show that several key environmental drivers control how dissolved TM behave in mangrove soils. In particular, (i) redox conditions, (ii) OM, and the (iii) mineralogy regulate whether metals remain bound to the solid phase or released into porewaters. As these factors vary along the land-sea gradient, each stand develops a specific biogeochemical signature, leading to distinct patterns of dissolved metal dynamics. While zonation emerged as the dominant explanatory factor in this study, other environmental drivers such as soil depth may also influence dissolved TM dynamics in mangrove soils (Deborde et al., 2015; Marchand et al., 2012; Noël et al., 2015).

4.2.1. Salt-flat: oxidizing conditions and low organic matter content

The salt-flat is characterized by well-oxygenated and alkaline conditions (Table 1; Mouras et al., 2025a), resulting from frequent desiccation cracks that facilitate oxygen diffusion into the soil. Its low tidal immersion, due to its highest position in the intertidal zone, further limits reducing processes, maintaining an overall oxic environment (Deborde et al., 2015; Marchand et al., 2012). TOC and DOC are minimal, reflecting limited organic inputs in this zone due to the absence of vegetation related to the high salinity (Mouras et al., 2025a). These physico-chemical conditions strongly influence partitioning of TM. Because redox potential controls the solubility of iron oxides, and pH modulates metal speciation and sorption capacity (Chakraborty and Babu, 2015; Liu et al., 2019; Sauvé et al., 1998), the high Eh and alkaline conditions of the salt-flat prevent the reductive dissolution of Fe(III) oxyhydroxides. This interpretation is supported by SEM-EDX observations showing that ilmenite grains in salt-flat samples display only rare dissolution features (Fig. 4a), together with the persistence of abundant Fe-oxide phases. Consistently, dissolved Fe concentrations remain low in salt-flat porewaters compared to the mangrove stands (Table 2), indicating limited reductive dissolution of Fe(III) oxyhydroxides under these oxidizing conditions. The elevated pH further may favour metal adsorption and precipitation, limiting the release of TM into the dissolved phase. Unlike reduced mangrove soils where Fe(III) oxyhydroxides dissolve and release associated TM (Zhu et al., 2018), such dissolution does not occur in this oxic zone, consistent with the lower dissolved Fe and Mn concentrations measured. Mineralogically, the salt-flat soils are dominated by Fe-Ti oxides (Ilmenites), as confirmed by SEM-EDX analyses (Fig. 4a). These oxides include Mn and sometime a low content of Cu. The attested presence of few ultramafic-derived grains, like chromite (Fig. S1), could also explain a part of the Cr, Ni and Co content of the samples. Nevertheless, the oxyhydroxides and clay minerals also present in the form of a thin coating around the quartz and felspars grains could, with the other oxides in a lesser extent, constitute the main adsorption sites for metals such as Ni, Cr, Co, and Zn. Indeed, under oxidizing conditions, Fe-oxide can adsorb other metals on their surfaces, thereby reducing their solubility (Lacerda et al., 2022). Similar behaviour of Fe-Ti oxides as major sorption phases has been documented in mangrove and ultramafic-influenced settings (Marchand et al., 2012). The high bulk density of the salt-flat reflect its sand-dominated soils dominated by the mineral fraction and low porosity, and further enhances metal retention. As a result, Fe, Ti, Ni, Co, and Cr stocks reach their maximum under the salt-flat (Table 4), consistent with previous observations in semi-arid mangroves of New Caledonia (Marchand et al., 2016). Interestingly, despite these high solid-phase metal stocks, the salt-flat also exhibits the highest dissolved concentrations for several TM, including Al, V, Co, Ni, Zn, Rb, Sr, and Mo, relative to the *A. marina* and *R. stylosa* zones (Table 2). This apparent paradox likely results from the combined effects of strong evaporation and high salinity, exceeding 100 in this zone (Table 1), which increase ionic strength and promote competition between major cations and TM for adsorption sites, thereby enhancing metal desorption (Acosta et al., 2011; Miranda et al., 2022). This hypothesis is supported by the high dissolved/solid ratios for example for Ni, Zn, and Mo, indicating greater distribution of these metals into porewaters. Grain size may further contribute, as the sandier soils of the salt-flat offer limited surface area for sorption, facilitating the release of dissolved metals into porewaters.

Eventually, Fe remains largely stable under these conditions, consistent with the dominance of Fe-Ti oxides displaying at the micrometre scales only rare dissolution features and the low Fe/Ti ratios observed in dissolved phases. Indeed, under the salt-flat, the

transformation of iron oxyhydroxides into pyrite is not observed (Noël et al., 2014). Together, these characteristics explain why the salt-flat exhibits both the largest solid-phase metal stocks and the highest dissolved concentrations for specific TM, highlighting the combined role of mineralogy, salinity, and evaporation in controlling metal distribution in semi-arid mangroves.

4.2.2. *A. marina* stand: suboxic and organic-rich soils

The *A. marina* stand represents an intermediate position along the land-sea gradient in the Bouraké semi-arid mangrove. This intermediate position is reflected in metal stocks, which are generally between those measured in the landward salt-flat and the seaward *R. stylosa* stands (Table 4). Bulk density and porosity are influenced by the vegetation cover, which promotes fresh OM accumulation and finer soil, leading to moderate water retention (Mouras et al., 2025a; Table 1). Physico-chemical conditions in this stand are characterized by slightly acidic pH and moderately reducing redox potential compared to the salt-flat, resulting from frequent tidal inundation (Table 1). The presence of pneumatophores and root systems enhances oxygen diffusion, while bioturbation and crab burrows further contribute to localized oxygenation (Ferreira et al., 2007; Kristensen et al., 2008). These dynamics create suboxic to slightly reducing conditions, with numerous micro-environments displaying their specific characteristics. However, the overall reducing conditions are sufficient to reduce Fe(III) oxyhydroxides to soluble Fe(II), but not enough to promote extensive sulfide precipitation as observed under *R. stylosa* (Noël et al., 2014). Mineralogically, the soils contain Ilmenites similar to the salt-flat, but with lower abundance and displaying numerous dissolutions feature, and the presence of few pyrite formations, consistent with SEM-EDX observations (Fig. 4f). This mineral composition, coupled with the finer texture and moderate OM content, is consistent with enhanced retention of TM such as Ni, Co, Cr, Cu, and Zn in the solid phase (Table 3). At the same time, it may favour the release of Fe and Mn into porewaters (Table 2), likely through partial reductive dissolution of Fe-bearing oxide phases under suboxic conditions, as commonly described in mangrove soils (Noël et al., 2014; Taillefert et al., 2002; Thamdrup et al., 2000). Dissolved/solid ratios highlight an enhanced partitioning of Fe and Mn toward the dissolved phase, reflecting ongoing Fe-oxide reduction and metal release. The combination of moderate reducing conditions, OM, and active oxygen transport by roots influences metal distribution and bioavailability. Fe(II) and other reduced metals can be oxidized near roots, forming iron plaques and making metals accessible for plant uptake (MacFarlane et al., 2007; Robin et al., 2021; Thakur et al., 2016). Clay minerals and oxyhydroxide coatings are more pronounced and thicker in this stand compared to the salt-flat. This fact, combined with the increase of OM compound (diatoms biofilms, wood fragments, DOC…) is leading to a higher potential of dissolved metal adsorption in these soils.

4.2.3. *R. stylosa*: strongly reducing and organic-rich soils

The *R. stylosa* stand represents the most reducing environment along the Bouraké mangrove gradient (Table 1). This seaward zone shows the lowest bulk density, consistent with the accumulation of fine-grained and autochthonous OM, mostly derived from mangrove litter degradation and enriched in humic compounds (Mouras et al., 2025a). Coupled with twice daily tidal flooding, this organic enrichment enhances microbial respiration and promotes persistent anoxic conditions (Marchand et al., 2016, 2012). The highly dynamic nature of tidal immersion also induces strong short-term variability in pH and redox potential, driving alternating oxic-anoxic phases that regulate TM speciation and distribution (Noël et al., 2014). Under reducing conditions, Fe(III) oxyhydroxides are dissolved, releasing Fe(II) and TM initially bound to them (Zhu et al., 2018). This is reflected in the elevated Fe/Ti and Ni/Ti ratios measured in solid phases, which indicate the disappearance of Ilmenite (almost all dissolved) in favour of pyrite (FeS_2) neoformation. It will lead to Ti depletion and is consistent with sulfide mineralization described in New Caledonian mangroves conditions (Marchand et al., 2016, 2012; Noël et al., 2014). SEM-EDX analyses reveal the presence of framboidal pyrite enriched in Ni, and Cu in a lesser extent, indicating that part of the released metals becomes reincorporated into sulphide phases during microbial sulphate reduction. Such processes are well documented in mangrove soils, where high sulfate availability and anaerobic respiration favour Fe-S mineralization and long-term metal sequestration (Kristensen et al., 2017; Marchand et al., 2012; Morse and Luther, 1999; Nóbrega et al., 2013; Noël et al., 2014). Such sulfide formation efficiently removes dissolved metals from porewaters and contributes to long-term sequestration. In addition to sulfide incorporation, organic complexation also drives dissolved metal behaviour in this stand. Indeed, as observed in the SEM, the majority of the "sand grains" of these samples are complex organo-mineral aggregates (including wood fragments and diatoms biofilms), demonstrating the abundance and critical role of OM on the geochemical processes affecting this stand. In the PCA (Fig. 5), Mo and U are both associated with OM-rich and reduced samples, showing a strong positive correlation ($r = 0.88$). Despite this association, dissolved Mo concentrations are lowest under these reducing conditions (Table 2), likely due to the combined effects of sulfide precipitation, adsorption onto Fe oxides, and organic complexation that reduce its solubility (Alongi, 2021; Pan et al., 2016; Wichard et al., 2009). Organic complexation processes are particularly relevant in the seaward zone, where OM originates mainly from leaf litter degradation and is rich in tannin-like compounds (Mouras et al., 2025a). Wichard et al. (2009) demonstrated that Mo strongly binds to plant-derived polyphenols such as tannins, which can immobilize Mo under anoxic and organic-rich conditions typical of mangrove soil. Such mechanisms likely contribute to the observed enrichment of solid-phase Mo and U in the most reduced, organic-rich soils of Bouraké (Table.3) (Mouras et al., 2026). Despite local solid-phase enrichment in Fe, Ni, and other metals due to intense reduction and pyritization, total metal stocks remain relatively low compared to the landward zones because of the low bulk density and high porosity of the organic-rich sediments. Alternating tidal inundation drives rapid Fe and Mn redox cycling, leading to dissolution into porewaters followed by rapid re-precipitation or incorporation into sulfide phases (Noël et al., 2014). The resulting low dissolved/solid ratios for most metals reflect a highly dynamic system where dissolution-reprecipitation cycles operate continuously. Dissolved metals may also be exported from the soil to coastal waters through tidal pumping (Knoke et al., 2024; Mori et al., 2019; Sadat-Noori and Glamore, 2019; Xiao et al., 2023). Furthermore, recent findings at the same site showed that tidal stage significantly influences dissolved TM dynamics in *R. stylosa* porewaters, with some metals potentially exported laterally to surface waters during spring tides by tidal mixing (Mouras et al., 2026). Overall, *R. stylosa* soils combine strongly reducing conditions, high OM, and extensive pyritization, resulting in temporary metal distribution in porewaters but efficient sequestration of TM in sulfide minerals, with potential export to the lagoon through tidal processes.

5. Conclusion

This study shows that dissolved trace metal concentrations and dynamics in semi-arid mangrove is primarily governed by the interaction between redox conditions, organic matter quantity and mineralogical transformations. These drivers shape distinct geochemical environments along the intertidal gradient and generate the strong spatial heterogeneity observed in porewater metal concentrations. By specifically focusing on the dissolved phase in a pristine semi-arid system, our results provide new insights into the natural geochemical processes governing TM mobility in mangrove soils, beyond the anthropogenic contamination contexts more commonly investigated. In addition, mangrove stand zonation (species and tidal immersion duration), strongly influences soil physico-chemical conditions such as oxygenation, evaporation intensity and dissolved organic matter availability.

These stand-driven conditions control TM distribution and their partitioning between the dissolved and solid phases.

Along this gradient, each stand displays a characteristic geochemical signature. The landward salt-flat is the most oxidizing zone and contains the highest proportion of Fe-Ti oxides (Ilmenites) resulting in the largest solid-phase metal stocks. Despite these high stocks, several dissolved metals concentrations remain elevated in this zone, likely due to high salinity and reduced sorption capacity in sandy, evaporative soils. In contrast, the *A. marina* stand shows lower redox potentials, high organic-matter contents, and the greatest dissolved Fe, Mn, Ni and Co concentrations. These patterns point to active Ilmenite, also containing Mn, dissolution and intense organic-matter diagenesis, making this zone the main internal producer of dissolved metals. Seaward, the *R. stylosa* stand is more frequently flushed by tidal waters, displays the strongest pyritization, and exhibits both low dissolved metal concentrations and the lowest solid-phase stocks signals consistent with metal sequestration into sulfides and enhanced export toward coastal waters. Oxic conditions and Fe-Ti oxides promote metal retention, whereas increasing anoxia, higher organic matter availability, and the transition toward sulfidic mineral phases favour either metal release or sequestration depending on the balance between dissolution and pyritization. The elevated dissolved concentrations of Fe, Mn, Ni and Co therefore reflect internal processes, particularly intense in the *A. marina* stands.

Once mobilized into porewaters, metals may become bioavailable and bioaccumulated by plants, as shown in previous studies, but they can also be exported. The low solid-phase stocks in the *R. stylosa* stand support the idea of increased metal mobilization and export in this seaward zone. Dissolved metals represent a potentially exportable fraction through tidal pumping, as suggested by the tidal variability in porewater concentrations observed at this site. However, direct quantification of metal export fluxes through tidal mass balance or tracer-based approaches remains necessary to confirm this hypothesis. Integrating measurements of the dissolved phase with the environmental drivers controlling geochemical transformations is therefore essential for accurately evaluating metal cycling and export in mangrove ecosystems.

CRediT authorship contribution statement

Naïna Mouras: Writing – review & editing, Writing – original draft, Visualization, Methodology, Investigation, Formal analysis, Data curation, Conceptualization. **Maximilien Mathian:** Writing – review & editing, Formal analysis. **Sarah Louise Robin:** Writing – review & editing. **Hugues Lemonnier:** Writing – review & editing, Supervision, Investigation, Funding acquisition, Conceptualization. **Cyril Marchand:** Writing – review & editing, Validation, Supervision, Funding acquisition, Conceptualization.

Funding sources

This research was undertaken in the context of Naïna Mouras's doctoral studies at the University of New Caledonia. Complementary funding was provided through the PRESENCE project, with contributions from the Government of New Caledonia and its South and North Provinces.

Declaration of competing interest

The authors declare that they have no known competing financial interests or personal relationships that could have appeared to influence the work reported in this paper.

Acknowledgements

The authors would like to thank Kapeliele Gututauava (University of New Caledonia) for his valuable assistance during fieldwork and Chloé Factou (University of New Caledonia) for her help with laboratory analyses. The authors also thank Thierry for welcoming them onto his property in Bouraké.

Appendix A. Supplementary data

Supplementary data to this article can be found online at https://doi.org/10.1016/j.marpolbul.2026.119926.

Data availability

Data will be made available on request.

References

Acosta, J.A., Jansen, B., Kalbitz, K., Faz, A., Martínez-Martínez, S., 2011. Salinity increases mobility of heavy metals in soils. Chemosphere 85, 1318–1324. https://doi.org/10.1016/j.chemosphere.2011.07.046.

Adame, M.F., Reef, R., Santini, N.S., Najera, E., Turschwell, M.P., Hayes, M.A., Masque, P., Lovelock, C.E., 2021. Mangroves in arid regions: ecology, threats, and opportunities. Estuar. Coast. Shelf Sci. 248. https://doi.org/10.1016/j.ecss.2020.106796.

Alkhadher, S.A.A., Suratman, S., Mohd Sallan, M.I. bin, 2023. An evaluation of spatial and seasonal distributions of dissolved trace metals in the water of the natural wetlands. J. Environ. Manag. 345, 118464. https://doi.org/10.1016/j.jenvman.2023.118464.

Alongi, D.M., 2014. Carbon cycling and storage in mangrove forests. Annu. Rev. Mar. Sci. 6, 195–219. https://doi.org/10.1146/annurev-marine-010213-135020.

Alongi, D.M., 2021. Macro- and micronutrient cycling and crucial linkages to geochemical processes in mangrove ecosystems. J. Mar. Sci. Eng. 9, 456. https://doi.org/10.3390/jmse9050456.

Alongi, D.M., Tirendi, F., Dixon, P., Trott, L.A., Brunskill, G.J., 1999. Mineralization of organic matter in intertidal sediments of a tropical semi-enclosed delta. Estuar. Coast. Shelf Sci. 48 (4), 451–467. https://doi.org/10.1006/ecss.1998.0465.

Ball, M.C., 1980. Patterns of secondary succession in a mangrove forest of Southern Florida. Oecologia 44, 226–235. https://doi.org/10.1007/BF00572684.

Bayen, S., 2012. Occurrence, bioavailability and toxic effects of trace metals and organic contaminants in mangrove ecosystems: a review. Environ. Int. 48, 84–101. https://doi.org/10.1016/j.envint.2012.07.008.

Beliaeff, B., Bouvet, G., Fernandez, J.-M., David, C., Laugier, T., 2011. Guide pour le suivi de la qualité du milieu marin en Nouvelle-Calédonie, Programmes Guide du milieu marin et Zonéco. [Tome Nickel et Environnement]. https://doi.org/10.34928/t864-x785.

Bourgeois, C., Alfaro, A.C., Bisson, E., Alcius, S., Marchand, C., 2020. Trace metal dynamics in soils and plants along intertidal gradients in semi-arid mangroves (New Caledonia). Mar. Pollut. Bull. 156. https://doi.org/10.1016/j.marpolbul.2020.111274.

Canfield, D.E., 1989. Reactive iron in marine sediments. Geochim. Cosmochim. Acta 53, 619–632. https://doi.org/10.1016/0016-7037(89)90005-7.

Carignan, J., Hild, P., Mevelle, G., Morel, J., Yeghicheyan, D., 2001. Routine analyses of trace elements in geological samples using flow injection and low pressure on-line liquid chromatography coupled to ICP-MS: a study of geochemical reference materials BR, DR-N, UB-N, AN-G and GH. Geostand. Newslett. 25, 187–198. https://doi.org/10.1111/j.1751-908X.2001.tb00595.x.

Chakraborty, P., Babu, P.V.R., 2015. Environmental controls on the speciation and distribution of mercury in surface sediments of a tropical estuary, India. Mar. Pollut. Bull. 95, 350–357. https://doi.org/10.1016/j.marpolbul.2015.02.035.

Deborde, J., Marchand, C., Molnar, N., Patrona, L.D., Meziane, T., 2015. Concentrations and fractionation of carbon, iron, sulfur, nitrogen and phosphorus in mangrove sediments along an intertidal gradient (Semi-Arid Climate, New Caledonia). J. Mar. Sci. Eng. 3, 52–72. https://doi.org/10.3390/jmse3010052.

Donato, D.C., Kauffman, J.B., Murdiyarso, D., Kurnianto, S., Stidham, M., Kanninen, M., 2011. Mangroves among the most carbon-rich forests in the tropics. Nat. Geosci. 4, 293–297. https://doi.org/10.1038/ngeo1123.

Douillet, P., Ouillon, S., Cordier, E., 2001. A numerical model for fine suspended sediment transport in the southwest lagoon of New Caledonia. Coral Reefs 20, 361–372. https://doi.org/10.1007/s00338-001-0193-6.

Duke, N., Meynecke, J.-O., Dittmann, S., Ellison, A.M., Anger, K., Berger, U., Cannicci, S., Diele, K., Ewel, K.C., Field, C.D., Koedam, N., Lee, S.Y., Marchand, C., Nordhaus, I.,

Dahdouh-Guebas, F., 2007. A world without mangroves? Science 317 (5834), 41–42, 317, 83–83.
Fernandez, J.M., Ouillon, S., Chevillon, C., Douillet, P., Fichez, R., Gendre, R.L., 2006. A combined modelling and geochemical study of the fate of terrigenous inputs from mixed natural and mining sources in a coral reef lagoon (New Caledonia). Mar. Pollut. Bull. 52, 320–331. https://doi.org/10.1016/j.marpolbul.2005.09.010.
Ferreira, T.O., Otero, X.L., Vidal-Torrado, P., Macías, F., 2007. Effects of bioturbation by root and crab activity on iron and sulfur biogeochemistry in mangrove substrate. Geoderma 142, 36–46. https://doi.org/10.1016/j.geoderma.2007.07.010.
Giri, C., Ochieng, E., Tieszen, L.L., Zhu, Z., Singh, A., Loveland, T., Masek, J., Duke, N., 2011. Status and distribution of mangrove forests of the world using earth observation satellite data. Glob. Ecol. Biogeogr. 20, 154–159. https://doi.org/10.1111/j.1466-8238.2010.00584.x.
Holloway, C.J., Santos, I.R., Tait, D.R., Sanders, C.J., Rose, A.L., Schnetger, B., Brumsack, H.J., Macklin, P.A., Sippo, J.Z., Maher, D.T., 2016. Manganese and iron release from mangrove porewaters: a significant component of oceanic budgets? Mar. Chem. 184, 43–52. https://doi.org/10.1016/j.marchem.2016.05.013.
Kierczak, J., Pietranik, A., Pędziwiatr, A., 2021. Ultramafic geoecosystems as a natural source of Ni, Cr, and Co to the environment: a review. Sci. Total Environ. 755. https://doi.org/10.1016/j.scitotenv.2020.142620.
Knoke, M., Dittmar, T., Zielinski, O., Kida, M., Asp, N.E., de Rezende, C.E., Schnetger, B., Seidel, M., 2024. Outwelling of reduced porewater drives the biogeochemistry of dissolved organic matter and trace metals in a major mangrove-fringed estuary in Amazonia. Limnol. Oceanogr. 69, 262–278. https://doi.org/10.1002/lno.12473.
Kristensen, E., Bouillon, S., Dittmar, T., Marchand, C., 2008. Organic carbon dynamics in mangrove ecosystems: a review. Aquat. Bot. 89, 201–219. https://doi.org/10.1016/j.aquabot.2007.12.005.
Kristensen, E., Connolly, R.M., Otero, X.L., Marchand, C., Ferreira, T.O., Rivera-Monroy, V.H., 2017. Biogeochemical cycles: global approaches and perspectives. In: Mangrove Ecosystems: A Global Biogeographic Perspective: Structure, Function, and Services. Springer International Publishing, pp. 163–209.
Lacerda, L.D., Ward, R.D., Borges, R., Ferreira, A.C., 2022. Mangrove trace metal biogeochemistry response to global climate change. Front. For. Glob. Change. 5. https://doi.org/10.3389/ffgc.2022.817992.
Leopold, A., Marchand, C., Deborde, J., Allenbach, M., 2017. Water biogeochemistry of a mangrove-dominated estuary under a semi-arid climate (New Caledonia). Estuar. Coasts 40, 773–791. https://doi.org/10.1007/s12237-016-0179-9.
Liu, W., Jin, L., Xu, J., Liu, J., Li, Y., Zhou, P., Wang, C., Dahlgren, R.A., Wang, X., 2019. Insight into pH dependent Cr(VI) removal with magnetic Fe3S4. Chem. Eng. J. 359, 564–571. https://doi.org/10.1016/j.cej.2018.11.192.
Luz-Santos, T.T., Mounier, J.L.S., Marins, R.V., 2025. Complexing fluorescent dissolved organic matter (FDOM) along the Parnaíba River Delta, Northeast Brazil. Chemosphere 385, 144531. https://doi.org/10.1016/j.chemosphere.2025.144531.
MacFarlane, G.R., Koller, C.E., Blomberg, S.P., 2007. Accumulation and partitioning of heavy metals in mangroves: a synthesis of field-based studies. Chemosphere 69, 1454–1464. https://doi.org/10.1016/j.chemosphere.2007.04.059.
Man, K.-W., Zheng, J., Leung, A.P.K., Lam, P.K.S., Lam, M.H.-W., Yen, Y.-F., 2004. Distribution and behavior of trace metals in the sediment and porewater of a tropical coastal wetland. Sci. Total Environ. 327, 295–314. https://doi.org/10.1016/j.scitotenv.2004.01.023.
Marchand, C., Lallier-Vergès, E., Baltzer, F., Albéric, P., Cossa, D., Baillif, P., 2006. Heavy metals distribution in mangrove sediments along the mobile coastline of French Guiana. Mar. Chem. 98, 1–17. https://doi.org/10.1016/j.marchem.2005.06.001.
Marchand, C., Fernandez, J.M., Moreton, B., Landi, L., Lallier-Vergès, E., Baltzer, F., 2012. The partitioning of transitional metals (Fe, Mn, Ni, Cr) in mangrove sediments downstream of a ferralitized ultramafic watershed (New Caledonia). Chem. Geol. 300–301, 70–80. https://doi.org/10.1016/j.chemgeo.2012.01.018.
Marchand, C., Fernandez, J.M., Moreton, B., 2016. Trace metal geochemistry in mangrove sediments and their transfer to mangrove plants (New Caledonia). Sci. Total Environ. 562, 216–227. https://doi.org/10.1016/j.scitotenv.2016.03.206.
Maurizot, P., Robineau, B., Vendé-Leclerc, M., Cluzel, D., 2020. Introduction to New Caledonia: geology, geodynamic evolution and mineral resources. In: Geological Society Memoir. Geological Society of London, pp. 1–12. https://doi.org/10.6084/m9.figshare.c.4984385.
Miranda, L.S., Ayoko, G.A., Egodawatta, P., Goonetilleke, A., 2022. Adsorption-desorption behavior of heavy metals in aquatic environments: influence of sediment, water and metal ionic properties. J. Hazard. Mater. 421, 126743. https://doi.org/10.1016/j.jhazmat.2021.126743.
Mori, C., Santos, I.R., Brumsack, H.J., Schnetger, B., Dittmar, T., Seidel, M., 2019. Non-conservative behavior of dissolved organic matter and trace metals (Mn, Fe, Ba) driven by porewater exchange in a subtropical mangrove-estuary. Front. Mar. Sci. 6. https://doi.org/10.3389/fmars.2019.00481.
Morse, J.W., Luther, G.W., 1999. Chemical influences on trace metal-sulfide interactions in anoxic sediments. Geochim. Cosmochim. Acta 63, 3373–3378. https://doi.org/10.1016/S0016-7037(99)00258-6.
Mounier, S., Lacerda, L.D., Marins, R.V., Bemaim, J., 2001. Copper and mercury complexing capacity of organic matter from a mangrove mud flat environment, Sepetiba Bay, Brazil. Bull. Environ. Contam. Toxicol. 67, 0519–0525. https://doi.org/10.1007/s00128-001-0154-3.
Mouras, N., Marchand, C., Mathian, M., Lemonnier, H., 2025a. Seasonal Dynamics of Dissolved Organic Matter Along an Intertidal Gradient in Semi-arid Mangrove Soils (New Caledonia). https://doi.org/10.5281/ZENODO.17042320.
Mouras, N., Marchand, C., Mathian, M., Lemonnier, H., 2025b. Seasonal dynamics of dissolved organic matter along an intertidal gradient in semi-arid mangrove soils (New Caledonia). EGUsphere 2025, 1–41. https://doi.org/10.5194/egusphere-2025-4328.
Mouras, N., Marchand, C., Mathian, M., Factou, C., Mounier, S., Lemonnier, H., 2026. Vertical and tidal variability of dissolved organic matter in mangrove soils: influence on dissolved trace metal dynamics. Estuar. Coast. Shelf Sci. 333, 109785. https://doi.org/10.1016/j.ecss.2026.109785.
Nath, B., Birch, G., Chaudhuri, P., 2013. Trace metal biogeochemistry in mangrove ecosystems: a comparative assessment of acidified (by acid sulfate soils) and non-acidified sites. Sci. Total Environ. 463–464, 667–674. https://doi.org/10.1016/j.scitotenv.2013.06.024.
Nóbrega, G., Ferreira, T., Romero, R.E., Marques, A.G., Otero, X., 2013. Iron and sulfur geochemistry in semi-arid mangrove soils (Ceará, Brazil) in relation to seasonal changes and shrimp farming effluents. Environ. Monit. Assess. 185. https://doi.org/10.1007/s10661-013-3108-4.
Noël, V., Marchand, C., Juillot, F., Ona-Nguema, G., Viollier, E., Marakovic, G., Olivi, L., Delbes, L., Gelebart, F., Morin, G., 2014. EXAFS analysis of iron cycling in mangrove sediments downstream a lateritized ultramafic watershed (Vavouto Bay, New Caledonia). Geochim. Cosmochim. Acta 136, 211–228. https://doi.org/10.1016/j.gca.2014.03.019.
Noël, V., Morin, G., Juillot, F., Marchand, C., Brest, J., Bargar, J.R., Muñoz, M., Marakovic, G., Ardo, S., Brown, G.E., 2015. Ni cycling in mangrove sediments from New Caledonia. Geochim. Cosmochim. Acta 169, 82–98. https://doi.org/10.1016/j.gca.2015.07.024.
Otero, X.L., Ferreira, T.O., Huerta-Díaz, M.A., Partiti, C.S.M., Souza, V., Vidal-Torrado, P., Macías, F., 2009. Geochemistry of iron and manganese in soils and sediments of a mangrove system, Island of Pai Matos (Cananeia — SP, Brazil). Geoderma 148, 318–335. https://doi.org/10.1016/j.geoderma.2008.10.016.
Ouillon, S., Douillet, P., Lefebvre, J.P., Le Gendre, R., Jouon, A., Bonneton, P., Fernandez, J.M., Chevillon, C., Magand, O., Lefèvre, J., Le Hir, P., Laganier, R., Dumas, F., Marchesiello, P., Bel Madani, A., Andréfouët, S., Panché, J.Y., Fichez, R., 2010. Circulation and suspended sediment transport in a coral reef lagoon: the south-west lagoon of New Caledonia. Mar. Pollut. Bull. 61, 269–296. https://doi.org/10.1016/j.marpolbul.2010.06.023.
Pan, Y., Koopmans, G.F., Bonten, L.T.C., Song, J., Luo, Y., Temminghoff, E.J.M., Comans, R.N.J., 2016. Temporal variability in trace metal solubility in a paddy soil not reflected in uptake by rice (Oryza sativa L.). Environ. Geochem. Health 38, 1355–1372. https://doi.org/10.1007/s10653-016-9803-7.
Pérez, A., Cebrián-Torrejón, G., Montoya, N., Piquero-Cilla, J., Sanders, C.J., Doménech-Carbó, A., Machado, W., 2021. Organic matter redox state driven by specific sources in mangrove sediments: a case study from peruvian ecosystems. J. Mar. Sci. Eng. 9. https://doi.org/10.3390/jmse9121438.
Robin, S.L., Marchand, C., Ham, B., Pattier, F., Laporte-Magoni, C., Serres, A., 2021. Influences of species and watersheds inputs on trace metal accumulation in mangrove roots. Sci. Total Environ. 787, 147438. https://doi.org/10.1016/j.scitotenv.2021.147438.
Sadat-Noori, M., Glamore, W., 2019. Porewater exchange drives trace metal, dissolved organic carbon and total dissolved nitrogen export from a temperate mangrove wetland. J. Environ. Manag. 248. https://doi.org/10.1016/j.jenvman.2019.109264.
Sallan, M.I.B.M., Al-Hazmi, H.E., Suratman, S., Alkhadher, S.A.A., Szeląg, B., Majtacz, J., Kowal, P., Kurniawan, T.A., Piechota, G., 2023. Anthropogenic trace metals in Setiu Wetland: spatial and seasonal distribution and implications for environmental health. J. Water Process Eng. 55, 104172. https://doi.org/10.1016/j.jwpe.2023.104172.
Sanders, C.J., Santos, I.R., Maher, D.T., Sadat-Noori, M., Schnetger, B., Brumsack, H.-J., 2015. Dissolved iron exports from an estuary surrounded by coastal wetlands: can small estuaries be a significant source of Fe to the ocean? Mar. Chem. 176, 75–82. https://doi.org/10.1016/j.marchem.2015.07.009.
Sauvé, S., McBride, M., Hendershot, W., 1998. Soil solution speciation of Lead(II): effects of organic matter and pH. Soil Sci. Soc. Am. J. 62, 618–621. https://doi.org/10.2136/sssaj1998.03615995006200030010x.
Taillefert, M., Hover, V.C., Rozan, T.F., Theberge, S.M., Luther, G.W., 2002. The influence of sulfides on soluble organic-Fe(III) in anoxic sediment porewaters. Estuaries 25, 1088–1096. https://doi.org/10.1007/BF02692206.
Tardy, Y., Roquin, C., 1992. Geochemistry and evolution of lateritic landscapes. In: Developments in Earth Surface Processes. Elsevier, pp. 407–443. https://doi.org/10.1016/B978-0-444-89198-3.50021-0.
Taylor, S., McLennan, S., 1985. The Continental Crust: Its Composition and Evolution. Blackwell Scientific Publications, Oxford.
Thakur, S., Singh, L., Wahid, Z.A., Siddiqui, M.F., Atnaw, S.M., Din, M.F.M., 2016. Plant-driven removal of heavy metals from soil: uptake, translocation, tolerance mechanism, challenges, and future perspectives. Environ. Monit. Assess. 188, 206. https://doi.org/10.1007/s10661-016-5211-9.
Thamdrup, B., Rosselló-Mora, R., Amann, R., 2000. Microbial manganese and sulfate reduction in black sea shelf sediments. Appl. Environ. Microbiol. 66, 2888–2897. https://doi.org/10.1128/AEM.66.7.2888-2897.2000.
Thanh-Nho, N., Marchand, C., Strady, E., Van Vinh, T., Taillardat, P., Cong-Hau, N., Nhu-Trang, T.T., 2020. Trace metal dynamics in a tropical mangrove tidal creek: influence of porewater seepage (Can Gio, Vietnam). Front. Environ. Sci. 8. https://doi.org/10.3389/fenvs.2020.00139.
Ullmann, C.V., Campbell, H.J., Frei, R., Korte, C., 2014. Geochemical signatures in Late Triassic brachiopods from New Caledonia. N. Z. J. Geol. Geophys. 57, 420–431. https://doi.org/10.1080/00288306.2014.958175.
Wichard, T., Mishra, B., Myneni, S.C.B., Bellenger, J.-P., Kraepiel, A.M.L., 2009. Storage and bioavailability of molybdenum in soils increased by organic matter complexation. Nat. Geosci. 2, 625–629. https://doi.org/10.1038/ngeo589.
Xiao, K., Zhang, P., Santos, I.R., Wang, J.J., Li, Z., Wang, X., Wang, Y.H., Lu, M., Zhang, L., Li, H., 2023. Tidal pumping controls dissolved organic matter properties

and outwelling from mangrove groundwater to coastal water. Water Resour. Res. 59. https://doi.org/10.1029/2022WR033913.
Zhu, Y., Liu, J., Goswami, O., Rouff, A.A., Elzinga, E.J., 2018. Effects of humic substances on Fe(II) sorption onto aluminum oxide and clay. Geochem. Trans. 19, 3. https://doi.org/10.1186/s12932-018-0048-5.
Zhu, C.Q., Ghoto, K., Gao, G.F., Chen, J., Hu, W.J., Qiao, F., Liu, J.Y., Zheng, H.L., 2019. Trace metals complexation behavior with root exudates induced by salinity from a mangrove plant Avicennia marina (Forsk.) Vierh. Biorem. J. 23, 82–93. https://doi.org/10.1080/10889868.2019.1602108.